Carderock Division
Naval Surface Warfare Center

Philadelphia, PA 19112-5083

CARDIVNSWC-TR-62-00-09   November 2000

Survivability, Structures, and Materials Directorate
Technical Report

Mechanisms of Military Coatings Degradation— End of Fiscal Year 2000 Report

by

Anthony Eng
Forrest Pilgrim
Malay Patel

DTIC QU

20001212 006

Mechanisms of Military Coatings Degradation— End of Fiscal Year 2000 Report

by

Anthony Eng
Forrest Pilgrim
Malay Patel

REPORT DOCUMENTATION PAGE

Form Approved
OMB No. 0704-0188

1 AGENCY USE ONLY (Leave blank)	2. REPORT DATE November 2000	3 REPORT TYPE AND DATES COVERED Research and Development

4. TITLE AND SUBTITLE Mechanisms of Military Coatings Degradation—End of Fiscal Year 2000 Report	5. FUNDING NUMBERS
6 AUTHOR(S) Anthony Eng, Forrest Pilgrim, Malay Patel	

7 PERFORMING ORGANIZATION NAME(S) AND ADDRESS(ES) Carderock Division, Code 624 Naval Surface Warfare Center Naval Business Center Philadelphia, PA 19112-5083	8 PERFORMING ORGANIZATION REPORT NUMBER CARDIVNSWC TR-62-00-09

9. SPONSORING/MONITORING AGENCY NAME(S) AND ADDRESS(ES) SERDP POC: Army Research Laboratory (S. McKnight) Aberdeen, MD 21005	10. SPONSORING/MONITORING AGENCY REPORT NUMBER

11 SUPPLEMENTARY NOTES

12a. DISTRIBUTION/AVAILABILITY STATEMENT Approved for public release; distribution is unlimited.	12b DISTRIBUTION CODE A

13. ABSTRACT (Maximum 200 words)

Although many distinguished scientists have studied the mechanisms of coating degradation and their relationship to service life, the need still exists to identify and elucidate these mechanisms in state-of-the-art military coating systems. Once accomplished, a predictive service life and life cycle cost can be optimally determined. In order to leverage this significant body of research and to comply with the multi-facility, tri-service, and academia-coordinated effort under the current Strategic Environmental Research and Development (SERDP) Mechanisms of Military Coatings Degradation task, Naval Surface Warfare Center, Carderock Division (NSWCCD), Code 624 will identify and characterize degradation in candidate military coating systems. The characterization will include accelerated-laboratory, static-field, and dynamic-field exposures via dynamic mechanical thermal analysis and density. In order to identify and conceptualize the mechanisms of degradation and to develop predictive service life models, the NSWCCD research will be combined with research at the Army Research Laboratory (ARL), the State University of New York at Stonybrook (SUNY), and the Naval Air Warfare Center (NAWC). ARL and SUNY are investigating chemical, transport, spectroscopic, and surface morphological phenomena, while NAWC is analyzing electrochemical and adhesion effects. A significant amount of data pertaining to the physical and thermal/mechanical properties at ambient laboratory conditions, as well as with the accelerated and static field exposures has now been collected and analyzed. Based on the duration of the exposures to date, curing effects rather than degradation effects have been observed and characterized.

14. SUBJECT TERMS Tri-Service, SERDP, CARC, Low VOC, Coatings Degradation, Modulus, Glass Transition	15. NUMBER OF PAGES 56
	16. PRICE CODE

17 SECURITY CLASSIFICATION OF REPORT Unclassified	18. SECURITY CLASSIFICATION OF THIS PAGE Unclassified	19. SECURITY CLASSIFICATION OF ABSTRACT Unclassified	20 LIMITATION OF ABSTRACT Unclassified

CONTENTS

FIGURES

TABLES

ABSTRACT

Although many distinguished scientists have studied the mechanisms of coating degradation and their relationship to service life, the need still exists to identify and elucidate these mechanisms in state-of-the-art military coating systems. Once accomplished, a predictive service life and life cycle cost can be optimally determined. In order to leverage this significant body of research and to comply with the multi-facility, tri-service, and academia-coordinated effort under the current Strategic Environmental Research and Development (SERDP) Mechanisms of Military Coatings Degradation task, Naval Surface Warfare Center, Carderock Division (NSWCCD), Code 624 will identify and characterize degradation in candidate military coating systems. The characterization will include accelerated-laboratory, static-field, and dynamic-field exposures via dynamic mechanical thermal analysis and density. In order to identify and conceptualize the mechanisms of degradation and to develop predictive service life models, the NSWCCD research will be combined with research at the Army Research Laboratory (ARL), the State University of New York at Stonybrook (SUNY), and the Naval Air Warfare Center (NAWC). ARL and SUNY are investigating chemical, transport, spectroscopic, and surface morphological phenomena, while NAWC is analyzing electrochemical and adhesion effects. A significant amount of data pertaining to the physical and thermal/mechanical properties at ambient laboratory conditions, as well as with the accelerated and static field exposures has now been collected and analyzed. Based on the duration of the exposures to date, curing effects rather than degradation effects have been observed and characterized.

ADMINISTRATIVE INFORMATION

BACKGROUND

Military coatings, like industrial and automotive coatings, must possess a high level performance with respect to physical, mechanical, chemical, and optical properties, so as to function as an effective and durable system in a potentially harsh environment for a finite period of time (typically 5 – 10 years for aircraft, 10 – 20 years for ground vehicles and support equipment). However, unlike their commercial counterparts, military coatings also must satisfy predefined tactical requirements, such as low observability and chemical agent resistance, without the durability enhancing benefits offered by a clear coat, which is typically used in the automotive industry, or a resin rich surface used in high gloss commercial aircraft coatings. In general, military topcoats contain binders that are composed of polyester polyols crosslinked with polyisocyanates, whereas the research and usage of commercial clear coats has typically been based on acrylic-melamine and acrylic-urethane systems. Tactical requirements place additional performance constraints on military coatings, since these requirements normally require an increased pigment volume concentration to produce a high porosity/profile surface for low gloss (minimized observability) and/or a highly crosslinked polymeric structure to enhance resistance to tactically aggressive chemicals (i.e., thickened mustard [HD], soman [GD], and sarin [GB] nerve agents). Each of these compositional material characteristics tends to increase the susceptibility of military paints to brittle failure.

While significant differences clearly exist between military and commercial coating systems, to validate the initiation of the current research and development effort, much of the recent coating degradation research provides insightful data about similar polymer material compositions and characterization techniques as a starting point and reference for the current research with military systems. For instance, Bauer has indicated that all of the polymeric materials usually used in coatings are susceptible to UV light induced free radical oxidation and that crosslink scission via free radical attack was found to be proportional to the photo-oxidation rate in urethane crosslinked coatings.[1] Glass transition temperature (T_g) as described by Hill[2] is a "unifying basic concept concerning the behavior of polymeric materials which help to systematize mechanical property data" and "it is difficult to overemphasize the importance of T_g in determining the mechanical properties of coatings." Glass transition temperature along with density have both been shown to be relevant and sensitive indicators of degradation, and both tend to increase

when subjected to accelerated aging.[3-5] Nichols and Darr stated that the "majority of chemical changes that can occur in clear coats during weathering produce polar groups [which] allows for increased hydrogen bonding in the polymer matrix giving rise [...] to the often observed increase in T_g [and that] weathering progresses [and] chemical aging can also cause densification and occurs when the polymer undergoes chemical composition changes, due to degradation or continued curing, over the course of time." Rodgers et al.[6] concluded that changes to T_g via water/acid absorption involve a non-reversible chemical reaction and that the onset T_g decreases as this exposure time increases. Furthermore, color change and rate of reduction in gloss in organic coatings is a function of both the binder and the pigmentation[7] and is widely accepted to be exacerbated by exposure to weathering. In certain military and commercial situations, change in optical appearance alone is sufficient for declaring the need to repaint or overcoat.

Although the mechanisms of coating degradation and their relationship to service life have been studied by many distinguished scientists,[1,3,4,6-18] the need still exists to identify and elucidate the mechanisms of coating degradation in state-of-the-art military coating systems, so that predictive service life and life cycle cost can be optimally determined. In order to leverage this significant body of research and to comply with the multi-facility, tri-service, and academia coordinated effort under the current Strategic Environmental Research and Development Program (SERDP) Mechanisms of Military Coatings Degradation project, Naval Surface Warfare Center, Carderock Division will identify and characterize degradation in the candidate military coating systems after accelerated laboratory, static field, and dynamic field exposures via glass transition, density, gloss, and color. This information will be combined with the chemical/transport/spectroscopic/surface morphological data generated at the Army Research Laboratory/State University of New York at Stonybrook, and with the electrochemical/adhesion results produced by the Naval Air Warfare Center at Patuxent River to identify and conceptualize the mechanisms of degradation and to then develop predictive service life models.

EXPERIMENTAL

Materials

The samples used for testing were prepared in two general configurations:

(1) As a free film using one mil thick low surface tension Tedlar polyvinyl fluoride (DuPont Inc, Buffalo, NY) release film

(2) As a painted stainless steel mesh composite film

The candidate coating systems were applied via conventional air-atomized spray equipment or high volume, low-pressure (HVLP) equipment onto the selected substrates. The master sheet of free films was produced as approximately 6"x8" films. The use of free films, although appropriate for laboratory investigations of coating transitions via dynamic mechanical thermal analysis (DMTA), is less than optimum for field evaluations due to durability and retrieval issues. Fortunately, the use of a wire mesh supporting substrate[19-22] for the determination of T_g via DMTA has been shown to be effective with high resolution, such that the effects of aging can be successfully investigated. The characteristics of the stainless steel mesh substrate (Sefar America Inc, Kansa City, MO) are as follows: wire diameter of 76 µm (0.003 inch), 280 by 280 µm (0.0011 by 0.0011 inch) cell size, and 90 by 90 wires per inch. These physical mesh properties result in a sample film thickness of 155 µm (0.0061 inches).

Four coating systems are included in this study, as described below in Table 1.

Table 1: Coating Systems

Coating System	Topcoat	Primer	Primary Application
A	MIL-C-46168	MIL-P-53022	Army and USMC CARC coating system
B	MIL-C-64159 TYII	MIL-P-53030	Water reducible CARC (WRCARC) coating system
C	MIL-C-85285	MIL-P-23377	Solvent-based Aerospace system
D	ZVOC-TC	MIL-P-85582	Water-based Aerospace system

Typical coating performance properties (i.e., abrasion resistance, accelerated weathering resistance, flexibility, gloss, adhesion, viscosity profile, etc.) are detailed in a Strategic Environmental Research and Development Project Report.[23] This report generally shows that the WRCARC is either equivalent to or superior to the standard MIL-C-46168 coating. The current evaluation focuses on the camouflage green version of these coatings (conforming to FED-STD-595 color #34094). The primers utilized included a solvent-borne and a water-borne coating—conforming to MIL-P-53022 and MIL-P-53030, respectively. These primers are devoid of hazardous lead and chromate pigments.

Henceforth, the following nomenclature will be used to designate among the various coating systems and substrates: **"Designator"-"Coating"-"Substrate"**; where "Designator" refers to whether the coating comes from system A, B, C, or D (see Table 1), "Coating" refers to the topcoat (TC), primer (Pr), or the complete system (Sys), and "Substrate" refers to either free film (FF), or wire mesh (Mesh). For example, B-TC-Mesh will be used to refer to the MIL-C-64159 TYII topcoat that has been applied to a wire mesh substrate; D-Sys-FF refers to a free film composite of the ZVOC-TC with MIL-P-85582 primer.

The mesh substrates were coated with the coating *system* (primer plus topcoat). As a result, and especially in the cases where individual glass transition temperatures for the primer and topcoat are sufficiently different, two distinct tanδ peaks sometimes occurred—one corresponding to the primer and the other corresponding to the topcoat. In other cases, a somewhat distorted tanδ peak occurred, where the tanδ responses for the primer and topcoat partially merged, resulting in a "hump" or "shoulder," prior to the primary tanδ peak. And in yet other cases, where the T_g values are very close, no secondary peak or "shoulder" was present at all.

DMTA was performed following accelerated weathering of the coating specimens. GM9540 and QUV testing were performed at Army Research Laboratories (ARL), and ASTM B-117 testing was conducted at Naval Air Warfare Center, Aircraft Division, Patuxent River, MD (NAWCADPAX).

This study examines the effect of various types of static exposures on glass transition temperature, modulus, and cross-link density. Static exposure took place at NSWCCD in Philadelphia, PA (industrial setting), Atlas Weathering Services Group (AWSG) in New River, Arizona (desert setting), and AWSG in Miami, Florida (marine environment).

Density

Free-film samples were cut with a razor blade into approximately 3.175 mm x 3.175 mm (0.125" x 0.125") square paint chips. Due to the brittleness of the MIL-C-46168 free films, irregular shaped paint chips were often produced. Three paint chips were used to determine each of the density values. Relative density equilibrium was achieved when the paint chip (after gentle agitation) neither rose to the surface, nor sank to the bottom of an aqueous zinc chloride ($ZnCl_2$) solution in a standard flat-bottom, glass beaker. Deionized water and a concentrated aqueous $ZnCl_2$ solution were used to adjust the density of the solution

to this equilibrium point. The equilibrated solution was then transferred into an empty, pre-weighed Gay-Lussac pycnometer (25 $\pm$ 0.05 ml) to determine the accurate mass of the solution for the subsequent density determination. The Gay-Lussac specific gravity bottle or pycnometer, which conforms to ASTM D-369, is a high accuracy volumetric flask—due primarily to its capillary perforated stopper. The measurement accuracy of this method was determined by Nichols and Darr[4] to be $\pm$ 0.002 g/ml.

Dynamic Mechanical Thermal Analysis

Materials respond to an external stress or strain by storing energy elastically and/or by dissipating energy via the generation of heat. Materials that exhibit purely elastic behavior are governed by Hooke's Law, which states that the stress is directly proportional to the strain. The proportionality constant is known as the elastic or storage modulus (E'). Purely viscous materials are subject to Newton's Law, which states that the stress is directly proportional to the strain rate—the proportionality constant is the viscous or loss modulus (E''). Most materials exhibit both viscous and elastic properties and are, therefore, known as visco-elastic materials. Dynamic Mechanical Thermal Analysis (DMTA) is used to measure a material's response to an applied stress or strain. The dynamic (oscillatory) nature of DMTA results in a sinusoidal stress-strain relationship. It is convenient to define a complex modulus (E^*), which is a linear combination of the viscous (E'') and elastic (E') moduli. The ratio of the elastic modulus to the viscous modulus is known as the tanδ (tanδ = E''/E') or the loss tangent, and is an indicator of the damping properties of a material. In this project, E', E'', and tanδ values were measured as a function of temperature using DMTA via dynamic temperature ramp tests at an oscillation frequency of 1 Hz and a ramp rate of 3°C per minute. T_g was defined as the temperature corresponding to the peak of the loss tangent response.

DMTA is being used to characterize the CARC coating that is part of the coating degradation study. Properties determined via DMTA will include:

(1) Glass transition temperature
(2) Viscous and elastic modulus
(3) Crosslink density

All three properties will be determined, in whole or in part, by a DMTA procedure known as Dynamic Temperature Ramp (DTR). T_g and modulus data will follow directly from DMTA testing, per ASTM E 1640. Crosslink density (XLD) calculation will incorporate the DMTA data with the method of Hill[5].

DMTA Equipment

A Dynamic Mechanical Thermal Analyzer manufactured by Rheometric™ Scientific (Model DMTA IV) was used to determine modulus and glass transition data. The DMTA IV is a mechanical spectrometer that can measure stress-strain relationships of materials. A Test Module provides mechanical deformation and environmental control to the test specimen. The Test Module's thermal and mechanical behavior is controlled by an Electronics unit, which also collects data during testing. Sub-ambient temperature control is achieved via liquid nitrogen Cryogenic System.

RESULTS AND DISCUSSION

DMTA

The preliminary study included DMTA of pertinent primers, topcoats, and systems (primer with topcoat). These materials were studied as free films and over various substrates. The preliminary data is included in Table 2.

A Dynamic Temperature Ramp (DTR) Test was used to determine T_g—this consists of ramping the temperature at a given rate while measuring changes in the elastic and viscous moduli of the material. DTR tests were conducted at 3°C/min and 1 Hz.

In this report, the four coating systems are studied following ambient cure, accelerated aging, and static field exposure. Data obtained from the ambient cure (baseline) material is discussed with emphasis on the two substrate-types (free film, wire mesh). Free films and, to a lesser degree, mesh substrates will be discussed in the analysis of the accelerated and field exposures.

DMTA analysis was performed on the ambient-cure material at 2-, 6-, and 12-week intervals. The 6-week baseline material corresponds (approximately) to the initiation of accelerated (and static field) exposures; hence, the 6-week baseline data was chosen as a reference point (or pre-environmental exposure point) for comparison to the various accelerated and static field data. In the discussion that follows, "baseline" will refer to the 6-week, ambient-cure material.

"A": Solvent-Borne CARC, MIL-C-46168

The DTR plot corresponding to the A-TC-FF baseline at 2-, 6-, and 14-week cure durations is shown in Figure 1. T_g steadily decreases from 72°C to 66°C to 62°C, respectively. A slight (and most likely negligible) decrease in $tan\delta_{max}$ is also evident. The authors of this paper believe that the decrease in T_g associated with the MIL-C-46168 topcoat (although counter-intuitive) may be related to a plasticization effect (probably due to water absorption). The values for T_g are consistent with concurrent work being performed by scientists at ARL.

Due to the very slight change in the height of the $tan\delta$ peaks, which were thought to be negligible in the MIL-C-46168 topcoat, the majority of the curing detectable via DMTA is believed to have occurred prior to the initial two-week cure period. When evaluating similar coating types (formulated with much lower NCO/OH ratios), other researchers found that 97% (via IR-ATR spectroscopy) and complete isocyanate reaction (via XPS) had occurred within 7 days of application[24], which generally supports the cure data presented herein. The storage modulus in the glassy and rubbery regions for the A-TC-FF (Figure 1) remains relatively consistent throughout the three cure intervals.

DMTA has been performed at 3-, 6-, and 12-week intervals, following ASTM B-117, GM9540, and QUV accelerated aging. Figures 2 – 7 show $tan\delta$ and E' versus temperature. These $tan\delta$ and E' plots (from DTR tests) were examined for each exposure type. Invariably, the accelerated exposure resulted in an increase in T_g from the baseline material. The elevated temperatures (from ambient) associated with each accelerated exposure contributes to this initial increase in T_g. Figure 2 shows that T_g continues to increase with ASTM B-117 exposure time, whereas Figures 4 and 6 indicate that T_g remains essentially constant for the GM9540 and QUV exposures. In addition, the magnitude or height of $tan\delta_{max}$ decreases with ASTM B-117 and QUV exposure time—this can be indicative of additional curing[25]. $Tan\delta_{max}$ remains relatively constant, and E' levels off in the rubbery region (Figure 5), during the GM9540 exposure, suggesting minimal additional cure is occurring. The storage modulus data for the QUV exposure (Figure 7) also suggests additional curing—in the rubbery region (T $> \approx$ 100°C), the E' curve reaches a minimum and then begins to rise again with increasing temperature. This increase in E' may be a result of continued cure. A similar result is not seen for the ASTM B-117 exposure (Figure 3), but this could be because the maximum temperature was insufficient to make the effect evident.

DMTA was performed at 7- and 13-week intervals, following static field exposures at Atlas sites in Arizona (desert setting) and Florida (marine environment), and at NSWCCD in Philadelphia, Pennsylvania (industrial setting). Figures 8 – 13 depict $tan\delta$ and E' plots, corresponding to each static field exposure. The samples exposed at the Arizona and Florida Atlas sites exhibited an initial increase in T_g (Figures 8 and 10) compared to the 6-week baseline sample. After this initial increase, the Arizona samples maintained a relatively constant T_g after 13 weeks of exposure. The Florida material exhibited a further increase in T_g at 13 weeks. The T_g for the 7-week Pennsylvania samples did not increase, but an increase was observed for the 13-week material (Figure 12). Based on a stable T_g value, the Arizona material does not appear to be undergoing any additional cure under ambient laboratory conditions; however, the decreasing $tan\delta_{max}$ (Figure 8), coupled with a rising E' in the rubbery region (Figure 9), indicates that the material is becoming stiffer (less flexible), and that additional conversion is occurring at temperatures above T_g. This is consistent with the densification of the Arizona material (see Table 3). The Florida Atlas

material appears to be undergoing additional curing, as evidenced by increasing T_g, decreasing $\tan\delta_{max}$ (Figure 10), and increasing E' in the rubbery region (Figure 11). The Pennsylvania material increases slightly in glass transition temperature from the 7- to 13-week interval, but further cure and stiffening (densification) appear minimal—again consistent with the density data. Figure 13 is consistent with this analysis; E' is still increasing in the rubbery region at the 7-week measurement, but appears to have leveled off after the 13-week measurement. The overall effects of the various exposures on T_g and $\tan\delta$ are depicted in Figures 14 and 15, respectively.

"B": Water-Reducible CARC (WRCARC), MIL-C-64159 TYII

The DTR plot corresponding to the WRCARC topcoat free films at 2-, 6-, and 14-week ambient cure durations is shown in Figure 16—$\tan\delta$, E', and E" are shown. The glass transition temperatures for the WRCARC free films remain relatively consistent (93°C to 93°C to 95°C). Again, a slight decrease (probably negligible) in $\tan\delta_{max}$ (0.43 to 0.42 to 0.39) is observed. The consistent T_g values determined for the WRCARC system are considered indicative of the relative stability of this topcoat. As an example, undesirable property changes related to weathering or aging are often accompanied by a change in T_g.[26, 27] Researchers at ARL found similar trends in an earlier investigation of the solvent-based and water-reducible coating systems.[28, 29] In that investigation, the authors reported a downward shift in the T_g of the solvent-based system over a three-week ambient drying period of the free film, with no further changes over the remaining drying period of six months. The water reducible system; however, showed an increase in T_g over the first three weeks of the ambient drying period and an additional increase in T_g over the remaining drying period of 6 months.

Due to the very slight change in the height of the $\tan\delta$ peaks, which were thought to be negligible in the WRCARC topcoat, the majority of the curing detectable via DMTA is believed to have occurred prior to the initial two-week cure period. The storage modulus in the glassy and rubbery regions for the WRCARC topcoat remains relatively consistent throughout the three cure intervals.

The values of E' in the glassy region are indicative of the relative stiffness among different coatings. After a 6-week cure, the WRCARC free film exhibited a lower E' in the glassy region (-40°C to 40°C) than did the MIL-C-46168—roughly half a decade (5×10^9 Pa) difference. This difference in stiffness is expected to minimize the susceptibility of WRCARC to brittle failure. Impact-resistance and mandrel-bend tests corroborate that WRCARC possesses a high degree of flexibility compared to the MIL-C-46168.[23] This general flexibility difference is also clearly observed when preparing DMTA specimen and handling the two coating types.

The T_g of the WRCARC is approximately 30°C higher than that of the MIL-C-46168, and it occurs around 90°C. Typical operational temperatures occur between 0°C and 60°C, and, as a result, the WRCARC is expected to exhibit enhanced dimensional stability when compared to the MIL-C-46168. The reason for this is straightforward. Thorough cure and sufficient stiffness are seemingly achieved with the WRCARC; therefore, the 30-degree temperature cushion or tolerance is expected to minimize the probability of degradation associated with increased polymer chain mobility in the transition region.

Free films of the WRCARC (B-TC-FF) underwent ASTM B-117, GM9540, and QUV accelerated exposure testing. In all cases, this material exhibited an increase in T_g (from the baseline sample) and then remained relatively stable at the 3-, 6-, and 12-week intervals. Figures 17 – 22 depict $\tan\delta$ and E' plots for these exposures. As depicted in Figures 17 and 19, tan data for the ASTM B-117 and GM9540 exposures is very consistent; the curves for the 3-, 6-, and 12-week measurements are virtually indistinguishable. It appears curing is complete following the initial exposure period. QUV exposure also resulted in stable (essentially constant) T_g values (Figure 21). The height of the tan peak increased with exposure time, and, while this would indicate the absence of additional curing, this effect is not yet completely understood. E' data from DTR tests is shown in Figures 18, 20, and 22, and indicates that no additional cure is occurring above T_g.

For the static field exposures, glass transition temperatures have been measured after 7- and 13-week exposures. DMTA plots are provided as Figures 23 – 28. The 7-week T_g values all increased slightly from the baseline value (Figures 23, 25, and 27). The Arizona and Pennsylvania samples exhibited a relatively constant T_g when measured at 13 weeks; no additional cure is evident (confirmed by E data depicted in Figures 24 and 28). The 13-week Florida material showed an increase in T_g (from 98°C to 107°C), indicating significant conversion occurred between the 7- and 13-week measurements. However, based on the increase in $tan\delta_{max}$ (Figure 25) and the level (or slightly decreasing) E' in the rubbery region (Figure 26), additional cure does not appear to be occurring at temperatures beyond T_g. It is feasible that the high humidity environment at the Florida site is (at least partially) responsible for the noted increases in glass transition temperature. The phenomenon is not seen at the other, less humid, sites. Figures 29 and 30 are scatter plots showing the overall effects of the exposures on T_g and $tan\delta_{max}$, respectively.

"C": Solvent-Based Aerospace system, MIL-C-85285

As cure increases from 2 to 6 to 14 weeks at ambient laboratory conditions for the C-TC-FF, T_g steadily decreases from about 39 to 34 to 30°C while the tan δ peak value, breadth, and general shape remain essentially constant as shown in Figure 31 and Table 2. Although the glass transition trend is decreasing and thus initially counter-intuitive, it appears to be a real and significant effect and will be discussed in greater detail later in this report. This decreasing trend is similar to that of the A-TC-FF data, since both of these coatings decrease by about 10° for up to 14 weeks at ambient cure conditions. Since both Coatings A and C are polyester polyol/hexamethylene diisocyanate-based solvent-borne polyurethanes with similar NCO/OH ratio's (1.0-1.3) and both have glass transitions greater than the cure temperature, it is not unreasonable to think that the cure mechanism and T_g trends would be similar. The reactivity of the polymer, which is a function of the polyester molecular weight and degree of branching, probably produces the level of T_g value shown and also it's rate of cure.

E'_{min} in the rubbery region, which is directly related to the cross-link density, appears to primarily decrease (Figure 32). This is currently not explainable since cross-link density should not decrease unless bond scission occurs which is unlikely since degradation stressors are not present at ambient laboratory conditions. The loss modulus expectedly maintains a consistent shape and follows the decreasing temperature trend observed for the loss tangent peaks.

Figures 33 – 46 depict DTR plots corresponding to the accelerated and static exposures for C-TC-FF. T_g was observed to slowly increase in the QUV, Florida and Pennsylvania tests (Figures 37, 41, and 43), while the T_g remained essentially constant in the ASTM B-117, GM9540, and Arizona exposure tests (Figures 33, 35, 39). These general trends in T_g are also displayed in a single scatter plot in Figure 45 and in Table 2. Since T_g can be directly related to degree of conversion and since vitrification is a reversible process (whereas gelation is irreversible),[30] this general increase and/or level glass transition response (versus a decrease at ambient conditions) is believed to be related to the curing of the polymer due to the energy (i.e., thermal, UV) imparted by these exposures. It is anticipated that the nearly level T_g response of the ASTM B-117, GM9540, and AZ exposures will increase as the duration progresses, at least partially due to the process of devitrification caused by the imposed energy.

The tan δ peak values for the C-TC-FF up to the 13-week exposure, as shown in the previous figures and in Figure 46 (scatter plot) displays a sharp decline in the QUV environment and a small decrease in the Arizona environment. This response is consistent with increasing drying and/or curing. The tan δ peak values over this same period shows a nearly constant response for GM9540, Florida, and Pennsylvania environments. This constant response in these three environments is indicative of the slow curing process when diffusion-controlled isothermal curing is dominant. A small but steady increase in the tan δ peak values for the ASTM B-117 condition was observed up to and including the 13week exposure period and may have been related to the constantly humid chamber conditions. The low temperature (-30 to +20°C) peak observed in the QUV environment at the 12 week interval, as shown in Figure 37, is thought to be an artifact of the test equipment/specimen and/or may have been due to grip slippage in the DMTA tensile fixture.

As shown in Figures 33, 35, 37, 39, 41, and 43, there is an obvious broadening of the loss tangent response in the QUV environment (particularly evident after the 12 week duration) and a very slight to imperceptible broadening in the other environments compared to the baseline. This seems to indicate that additional heterogeneous cross-links are being formed where significant thermal energy is imparted to the samples. Although the response in QUV seems appropriate, since the imparted continuous 60°C temperature of this chamber is significantly above the T_g, it can only be assumed that the lack of broadening of the loss tangent spectra in the GM9540 environment, which also introduces a 60°C low humidity (<30%RH) cycle, must be due to the lack of significant levels of moisture during this period of increased polymer mobility and free volume. When the GM9540 imparts higher levels of moisture (100% RH); however, the temperature is regulated to 25°C and thus mobility would be significantly decreased since T_{cure} would then be less than T_g.

The response of the C-TC-FF in the rubbery region for the E' spectra, which corresponds to the relative cross-link density of the film, was unexpectedly observed to generally decrease or remain about the same for all environments over the 3- to 13-week exposure periods—as indicated in Figures 34, 36, 38, 40, 42, and 44, and in an overall scatter plot as shown in Figure 46. To correlate the E'_{min} with the tan delta response spectra (i.e., peak height and width), we would have expected to see an increase in the cross-link density for the QUV environment but a negligible increase for all other exposures. Also, since cross-link density should increase or remain the same with increasing cure time unless polymer bond breakage occurs, it is suspected that this rubbery region storage modulus data are inappropriate/invalid for correlation to relative crosslink density for this thermal regime. Additional testing may resolve this issue.

"D": Water-Based Aerospace system, ZVOC-TC

As cure progresses from 2 to 6 to 14 weeks at ambient laboratory conditions for the ZVOC TC free film (D-TC-FF), the glass transition temperature continually decreases from about 48 to 41 to 36°C as displayed in Figure 47 and Table 2. This decreasing trend in T_g with increasing ambient cure duration is similar to that of the A and C coatings and will be discussed later in this report. It is an interesting side note that both A and C coatings are solvent-borne whereas coating D is water-borne. Apparently, the type of film formation (solution for solvent borne coating C versus coalescing for water-borne coating D) does not have an overwhelming effect on glass transition temperature, since both of these coatings have similar T_g's and T_g cure trends at these ambient conditions. It is probable; however, that if film formation would impart an effect, it would occur within the first 96 hours of cure. The loss tangent peak value, breadth, and general shape remain approximately constant.

The E'_{min} in the rubbery region (Figure 48) generally increases which indicates an increase in relative cross-link density. This appears to be a normal polymer curing/aging trend although the validity of this data has to be scrutinized since the trends for the previous coating (MIL-C-85285) were unexpected.

Figures 49 – 62 depict DTR data for accelerated and static exposures. As shown in Table 2 and Figures 49, 51, 53, 55, 57, and 59, the glass transition temperatures for the ZVOC TC (coating D) free film after conditioning from 3 to 13 weeks were observed to sharply increase for QUV and Florida exposures, generally increase for GM9540, and remain about constant for ASTM B-117, Arizona and Pennsylvania exposures. It should be noted that the 3 week spectra in the ATM B-117 environment (Figure 49) displays a small peak, probably due to contamination, at about 35°C, which apparently affects the primary peak (i.e., shifts it to a higher level) and thus should be considered anomalous. The trends for the current data are succinctly displayed on a scatter chart in Figure 61, which generally shows that T_g increases with exposure time as a sufficient amount of curing energy is transferred from the various test environments into the polymer. This, in essence, is the impetus for the increased polymer mobility/free volume and the subsequent devitrification process. Similar to the previous coating (MIL-C-85285) and based on the current data, it is expected that the T_g for the ASTM B-117, GM9540, Arizona, and Pennsylvania exposures will increase in subsequent testing.

The $tan\delta_{max}$ data for the ZVOC TC is clearly shown in the previous loss tangent spectra, and also in Figure 62 (scatter plot) as decreasing as the duration progresses for up to 13 weeks for all of the

8

environmental exposures. This trend correlates well with the accepted trend for the curing (and stiffening) of thermosets.[26] It should also be noted that unlike the tan δ max response for coating C in the ASTM B-117 exposure which exhibited an increasing response, the same property for coating D exhibited a decreasing response as exposure duration increased. This highlights a general response of coatings C versus D with respect to high moisture environments and stability in various environmental exposures which will be discussed further later in this report.

Tan δ response curves become broader as the exposure duration increases for the ZVOC TC as shown in Figures 49, 51, 53, 55, 57, and 59. The breadth is more substantial in the accelerated lab versus the static field exposures. This seems logical since the additional curing imparted by the accelerated chamber conditions would be expected to cause additional curing and potentially additional heterogeneous cross-links (i.e., isocyanate with water to form urea). Interestingly, there is a substantial broadening of the ASTM B-117 peak with a concurrent decrease in tan δ max with no apparent change in T_g and a lack of loss tangent width increase and a lack of a loss tangent intensity (height) change for the Florida exposure with a significant T_g increase. This may be better understood when the chemical analysis data from the other team members is generated and analyzed. Also, additional DMTA test data in the next fiscal year should allow for a better correlation of these characteristics.

The storage modulus in the rubbery zone (which can be correlated to the relative crosslink density) as shown in DMTA plots in Figures 50, 52, 54, 56, 58, and 60 is generally shown to be increasing during the 3- to 13-week exposure durations with two notable exceptions. The anomalous data were based on the GM9540 and QUV exposures. Both of these accelerated environmental exposures displayed sharp increases followed by sharp decreases in E'_{min} (i.e., cross-link density). This decrease in E' may be related to the melting of semi-crystalline domains present in random samples. This will be investigated further in the next fiscal year when additional data will be generated to more clearly characterize these responses.

Mesh Substrate: Coatings A, B, C, and D

The use of free films, although appropriate for DMTA analysis in the laboratory, may be less than optimum for field evaluations. Durability and retrieval issues could make free film analysis impractical. In this case, a rigid or semi-rigid substrate may be required. NSWCCD has obtained consistent T_g data for coatings applied to a stainless-steel-mesh substrate. T_g values measured for the MIL-C-46168 system (A-Sys-Mesh) varied from 66°C to 71°C when DMTA analysis was performed on the free film and on the wire mesh specimen, respectively. Figure 63 depicts a tanδ plot for the A-Sys-Mesh sample.

Good consistency was achieved with these configurations when measuring T_g of the WRCARC system (93° to 91°, respectively). Figure 64 depicts tanδ curves corresponding to DMTA analysis of the A-TC-FF and A-TC-Mesh. Although the tanδ$_{max}$ values are varied depending on the specimen type, these values appear to be significant and prominent enough to conduct comparative analysis within each specimen type. This will greatly increase the chances of producing T_g data from the field for subsequent aging and degradation analysis.

The DMTA responses for the A and B coating systems (primer + topcoat) on the stainless steel mesh specimen displayed single peaks as shown in Table 2 and Figures 63 and 65. The contribution of the primer and the topcoat to the loss tangent spectra produces a composite peak of diminished magnitude and broader width compared to the same coatings analyzed individually as free film specimen. This composite peak is due to the close proximity of the T_g of the primer and topcoat. The C and D coating systems on mesh, on the other hand, displayed two transition peaks as shown in Table 2 and Figures 66 and 67. The magnitude of the topcoat response in the dual peak spectra is the minor peak, whereas the major peak is the response of the primer. In general, the T_g and loss tangent maximum data generated in the mesh composite specimen is slightly depressed compared to the value for the uniform free film specimen. This discrepancy may be related to a perturbation caused by the presence of the primer and/or by an interaction caused by the wire cross-over junctions of the mesh. Despite this slight disparity, this data supports the trends in the glass transition temperature data described for the A, B, C, and D topcoat free films, in general. Since the

sensitivity of the loss tangent response for the topcoat in the mesh specimen is less than that for the free film, this data using the mesh specimen will not be discussed further in this report.

Overall Coating Effect

Based on the steady decrease in T_g at ambient laboratory conditions and the general reversal in T_g (after a distinct induction period) in the various accelerated laboratory and static field environmental exposures, it is probable that the trends observed for coatings A, C, and D were due to incomplete crosslinking of this polymer and the concomitant vitrification process. This is supported by work of others which indicated that the maximum degree of cure was generally shown to be less than complete due to a quenching of the thermoset reaction via vitrification where the isothermal curing temperature was less than the T_g.[31,32] While the isothermal cure temperature was significantly below the T_g for coatings A and B, it is important to note that although the T_g for coatings C and D were just above the isothermal cure temperature, it is thought that vitrification of these polymers nonetheless occurs. From a thermodynamic point of view, this vitrified material would not be in a state of equilibrium. These amorphous regions will try to attain equilibrium by decreasing volume, enthalpy and entropy.[33] This supports the increase in density via physical aging that is due to an increase in chain mobility and a resultant decrease in free volume. However, the diffusion-controlled curing process that occurs shortly after vitrification for many thermosets, will be a slow process at the current isothermal cure temperature. As an example, Prime has stated that the reaction rate typically decreases by 2-3 orders of magnitude after complete vitrification.[34] Thus after vitrification under the same ambient curing temperature, a leveling or inhibition of cure properties (i.e., glass transition temperature) should be evident. The decreased rate of change of coatings A, C, D between 6 and 14 weeks versus the decrease between 2 and 6 weeks at ambient laboratory conditions supports this inhibited cure mechanism due to vitrification.

Apparently, coating B did not undergo these same polymer realignment events or morphological changes to produce vitrification compared to those related to the glass transition changes observed for the A, C, and D coatings during the same time period at ambient conditions. Coating B on the other hand, exhibits a consistent T_g, which may be attributable to more thorough cure (higher degree) conversion and/or quicker cure (chemical and diffusion controlled). Potentially, the extremely high NCO/OH ratio of coating B may be the prominent factor in the curing of this coating. The extreme over indexing (NCO/OH=5.0) may significantly reduce the number of unreacted hydroxyl groups and any excess NCO groups probably react with moisture within the first 96 hours of cure. Hegedus, et al have shown that in a waterborne resin, isocyanate reacts with water within the first 3 days of cure.[35] Thus, the majority of primary (isocyanate/hydroxyl) and secondary reactions (isocyanate/water, isocyanate/urea, urethane/isocyanate) are probably completed before the first DMTA dynamic temperature ramp test at 2 weeks for this B coating. This is supported by the dynamic time sweep test with the DMTA as shown in Figures 68, 69, and 70, where the storage modulus increases to about 2.6×10^9 Pa after about 4 days at ambient laboratory conditions for the B coating and then remains essentially constant over the next 2 days. It is suspected that the majority of the vitrification process probably occurred prior to the first baseline test (at 2 weeks). It is thought (but not yet verified) that the degree of conversion at ambient laboratory conditions, which produced this greater degree of stability, for the B coating was significantly greater than the degree of conversion for the other coatings, since it produced essentially constant glass transition temperatures over the 14 week cure at ambient conditions. Although the T_g data for this B coating seem to suggest that additional curing occurs, this is not supported by the tan delta spectra which should become broader nor the tan delta max curves which should decrease (an indicator of stiffening).

As discussed previously, the T_g of all four topcoats (A through D) generally displayed an increasing or a relatively constant trend (from baseline values) after induction into the accelerated laboratory and static field exposure environments. This response in these environmental exposure tests seems to indicate that additional curing occurs (particularly since the ambient cure data was in sharp contrast to the current data) due to the chemical constituents and/or thermal energy imparted by these exposures. The tan δ max data as well as the shape of the loss tangent response, in general, supports this hypothesis. Additionally, it appears that both coatings A and B increase their degree of cure due to the presence of water with thermal energy potentially imparting a secondary effect. This is demonstrated by their greater T_g response in the ASTM B-117 and GM9540 tests compared to their response in the QUV

test. This is best seen by referring to Figures 14 and 29 (T_g scatter plots for A and B). In general, the static field tests for coatings A and B also support this effect regarding water and temperature. Intuitively, thermal energy would be expected to play the largest role in cure in this scenario although this data seems to contradict this standard rationale. This same effect was not universally observed for the C or D coatings in these exposures. At this point, it can only be stated that the Florida exposure appears to have a significant effect on the T_g and thus the degree of conversion of both the C and D coatings (and also in the A and B coatings).

Density

The paint density data is listed in Table 3 for 3- and 7-week ambient room temperature cured samples (listed as 0 wk exposure duration) as well as for samples that were exposed to accelerated laboratory and static field aging. This data is also graphically displayed in Figures 71 –74 for the sake of visualization of the overall trend in density response as cure and exposure duration increases. The WRCARC and the ZVOC TC, both of which are waterborne topcoats, display an increase or an increase followed by a leveling off in density as cure time and exposure duration progresses for all of the laboratory and static field exposures. This response conforms to the general theory of physical aging, which says that amorphous solids below their glass transition are not in thermodynamic equilibrium and densification (primarily via a decrease in volume) of the non-equilibrium amorphous state will occur in the attempt to achieve equilibrium.[36, 37]

The two solvent-borne coatings (MIL-C-46168 and MIL-C-8528) generally follow the physical aging theory mentioned above although the trends over the course of the cure and exposure durations were not as consistent as the trends for the two waterborne coatings. There were two exceptions to these general trends for these solvent-borne coatings. The MIL-C-85285 coating in the ASTM B-117 exposure displayed a steady decrease in density with increasing duration of exposure, which is opposite to the general trend. This deviation; however, can best be explained by the continuously moist environment of the ASTM B-117 test, which apparently plasticized and expanded the polymer matrix and/or inhibited the inherent thermodynamic activity related to physical aging. The other anomaly consisted of a slight decrease in density for the MIL-C-46168 topcoat cured at the ambient laboratory conditions from baseline 1 (3 wk) to baseline 2 (7 wk). This decrease (1.927 to 1.922 g/ml) should probably be considered negligible, since the difference is relatively small and the density of this paint is relatively close to the maximum density of a saturated aqueous zinc chloride solution (2.14 g/ml in cold water and 2.30 g/ml in hot water). This would tend to increase the inherent level of variability. After the second baseline density was determined (1.922 g/ml) for the MIL-C-46168 topcoat, which was prior to the initiation of the exposure testing, all of the exposures displayed increasing density with increasing exposure. The overall trends and variability in this test will be optimized when continued data collection occurs in the next fiscal year (FY-01).

SUMMARY/CONCLUSIONS

The DMTA spectra and Gay-Lussac density data for the ambient cured, accelerated laboratory exposure tests, and static field exposure tests, generated and discussed herein, does not indicate that degradation has occurred within the bulk polymer. These coating properties seem to be; however, characteristic of various initial degrees of curing and vitrification at ambient laboratory conditions and then additional curing upon exposure to the various exposure tests. Coatings A (MIL-C-46168), C (MIL-C-85285), and D (ZVOC TC) tended to be less stable at ambient laboratory conditions (based on the significant decrease in glass transition temperature) than coating B (MIL-C-64159). Upon introduction into the environmental exposures, all four of the test coatings (A, B, C, D) displayed a tendency toward increased curing. After exposure in the various accelerated laboratory and static field environments, water-borne coating B seemed to be more stable (based on cure characteristics) than solvent-borne coating A while solvent-borne coating C appeared to be more stable than water-borne coating D. Finally, although the focus of this effort was to characterize and/or develop models of degradation with these high performance solvent-borne and water-borne coatings, it should be noted that data have yet to be produced beyond the point equivalent to 25% of the total planned exposure duration. Thus, additional testing is expected to reinforce the trends in the current data and also provides increased opportunity to produce degradation in the bulk polymer of the current systems.

ACKNOWLEDGEMENT

REFERENCES

1. Bauer, D.R., "Chemical Criteria for Durable Automotive Topcoats," *J. Coat. Technol.*, Vol. 66, No. 835, Aug 1994.
2. Hill, L.W., "Mechanical Properties of Coatings," FSCT Series Coat. Technol., April 1987.
3. Hill, L.W., "Structure /Property Relationships of Thermoset Coatings," *J. Coat. Technol.*, Vol. 64, No. 808, May 1992.
4. Nichols, M.E. and Darr, C.A., "Effect of Weathering on the Stress Distribution and Mechanical Performance of Automotive Paint Systems," *J. Coat. Technol.*, Vol. 70, No. 885, Oct 1998.
5. Gallagher, P. K., "Thermoanalytical Instrumentation, Techniques, and Methodology," Chapter 1 in *Thermal Characterization of Polymeric Materials*, 2nd Ed., Vol. 1, Turi., E.A. (Ed.), Academic Press, Inc., San Diego, CA, p133-149, 1981.
6. Rodgers, W.R., Garner, D.P., and Cheever, G.D., "Study of the Attack of Acidic Solutions on Melamine-Acrylic Basecoat/Clearcoat Paint Systems," *J. Coat. Technol.*, Vol. 70, No. 877, Feb 1998.
7. Bauer, D.R., "Predicting In-Service Weatherability of Automotive Coatings: A New Approach," *J. Coat. Technol.*, Vol. 69, No. 864, Jan 97.
8. Gerlock, J.L., Bauer, D.R., Briggs, L.M., and Dickie, R.A., "A Rapid Method of Predicting Coating Durability Using Electron Spin Resonance," *J. Coat. Technol.*, Vol. 57, No. 722, March 1985.
9. Dickie, R.A., "Chemical Origins of Paint Performance", *J. Coat. Technol.*, Vol. 66, No. 834, July 1994.
10. Martin, J.W. and McKnight, M.E., "The Prediction of Service Life of Coatings on Steel, Part I: Procedure for Quantitative Evaluation of Coating Defects," *J. Coat. Technol.*, Vol.57, No. 724, May 1985.
11. Martin, J.W., Saunders, S.C., Floyd, F.L., and Wineburg, J.P., "Methodologies for Predicting the Service Lives of Coating Systems," *FSCT Series Coat. Technol.*, June 1996.
12. Nguyen, T., Hubbard, J.B., and Pommersheim, J.M., "Unified Model for the Degradation of Organic Coatings on Steel in a Neutral Electrolyte," *J. Coat. Technol.*, Vol. 68, No. 855, April 1996.
13. Skerry, B.S., Alavai,A., and Lindgren,K.I., "Environmental and Electrochemical Test Methods for the Evaluation of Protective Organic Coatings," *J. Coat. Technol.*, Vol. 60, No. 765, October 1988.
14. Skerry, B.S. and Simpson, C.H., "Combined Corrosion/Weathering Accelerated Testing of Coatings for Corrosion Control," *Proc. NACE Corrosion 91 Conf.*, Paper No. 412, Cincinnati, OH, March 1991.
15. Appleman, B.R., "Predicting Exterior Marine Performance of Coatings from Salt Fog: Two Types of Errors," *J. Prot. Coat. & Lin.*, Vol. 9, No. 10, October 1992.
16. Kendig, M. and Scully, J., "Basic Aspects of the Application of Electrochemical Impedance to the Life Prediction of Organic Coatings," *Proc. NACE Corrosion 89 Conf.*, Paper No. 32, New Orleans, LA, April 1989.
17. Leidheiser, H., Jr., "Mechanism of Corrosion Inhibition With Special Attention to Inhibitors in Organic Coatings," *J. Coat. Technol.*, Vol. 53, No. 678, July 1981.
18. McQueen, R.C., Miron, R.R., and Granata, R.D., "Method for Corrosion Inhibitor Mechanism Studies in Epoxy Coated Aluminum," *J. Coat. Technol.*, Vol. 68, No. 857, June 1996.
19. Burns, J.M., Auser, W.D., Gutierrez, M.L., and Karmin, M.L., *Proc. North Am. Therm. Anal. Soc. Conf.*, 13th, p 369-374, 1985.
20. Prime, R.B., *Proc. North Am. Therm. Anal. Soc. Conf.*, 17th, p 707-713, 1988.
21. Neag, C.M. and Prime, R.B., "Application of Time/Temperature Superposition Techniques to Powder Coating Cure," *J. Coat. Technol.*, Vol. 63, No. 797, June 1991.

22. Neag, M., Wilson, P., and Skerl, G., "Coating Characterization Using Multiple Techniques and Statistically Designed Experiments," *J. Coat. Technol.*, Vol. 66, No. 832, May 1994.
23. R.W. Katz, "Low Volatile Organic Compound (VOC) Chemical Agent Resistant Coating (CARC)" SERDP Project #PP 1056, Army Armament Research, Development & Engineering Center, April 2000, p. A-8 to A-15 and N8 to N12.
24. C.R. Hegedus, A.G.. Gilicinski, and A.J. Haney, "Film Formation Mechanism of Two-Component Waterborne Polyurethane Coatings," *J. Coat. Technol.*, Vol. 68, No. 852, January 1996, p. 59.
25. R.B. Prime, "Thermosets," Chapter 6 in Thermal Characterization of Polymeric Materials, 2nd Ed., Vol. 2, Turi, E.A. (Ed.), Academic Press, Inc., San Diego, CA, 1981.
26. L.W. Hill, "Structure Property Relationships of Thermoset Coatings," *J. Coat. Technol.*, Vol. 64, No. 808, May 1992, p. 32, 35.
27. M.E. Nichols and C.A. Darr, "Effect of Weathering on the Stress Distribution and Mechanical Performance of Automotive Paint Systems," *J. Coat. Technol.*, Vol. 70, No. 885, October 1998, p. 148.
28. J. A Escarsega, D. M. Crawford, J. L. Duncan, K. G. Chesonis, "Water-Reducible PUR Coatings For Military Applications," *Modern Paints and Coatings*, Vol 87, 1997, p. 21.
29. D. M. Crawford, J. A. Escarsega, "Dynamic Mechanical Analysis of Novel Polyurethane Coating for Military Applications", *Thermochimica Acta*, Vol. 357, July 2000, p. 161.
30. R.B. Prime, "Thermosets," Chapter 6 in Thermal Characterization of Polymeric Materials, 2nd Ed., Vol. 2, Turi, E.A. (Ed.), Academic Press, Inc., San Diego, CA, 1981, pp. 1497,1498.
31. Kenny, J.M., and Trivisano, A. (1991). *Polm. Eng. Sci.* 31, 1426-1433.
32. Kenny, J.M., Trivisano, A., Frigione, M.E., and Nicolais, L. (1992). *Thermochim. Acta* 199, 213-227.
33. R.B. Prime, "Thermosets," Chapter 6 in Thermal Characterization of Polymeric Materials, 2nd Ed., Vol. 2, Turi, E.A. (Ed.), Academic Press, Inc., San Diego, CA, 1981, p. 1417
34. R.B. Prime, "Thermosets," Chapter 6 in Thermal Characterization of Polymeric Materials, 2nd Ed., Vol. 2, Turi, E.A. (Ed.), Academic Press, Inc., San Diego, CA, 1981, p. 1624.
35. C.R. Hegedus, A.G.. Gilicinski, and A.J. Haney, "Film Formation Mechanism of Two-Component Waterborne Polyurethane Coatings," *J. Coat. Technol.*, Vol. 68, No. 852, January 1996.
36. R.B. Prime, "Thermosets," Chapter 6 in Thermal Characterization of Polymeric Materials, 2nd Ed., Vol. 2, Turi, E.A. (Ed.), Academic Press, Inc., San Diego, CA, 1981, pp. 1417-1418.
37. M.E. Nichols and C.A. Darr, "Effect of Weathering on the Stress Distribution and Mechanical Performance of Automotive Paint Systems," *J. Coat. Technol.*, Vol. 70, No. 885, October 1998, p. 145.

Figure 1: DTR, Mil-C-46168, Free Film
Ambient Exposure
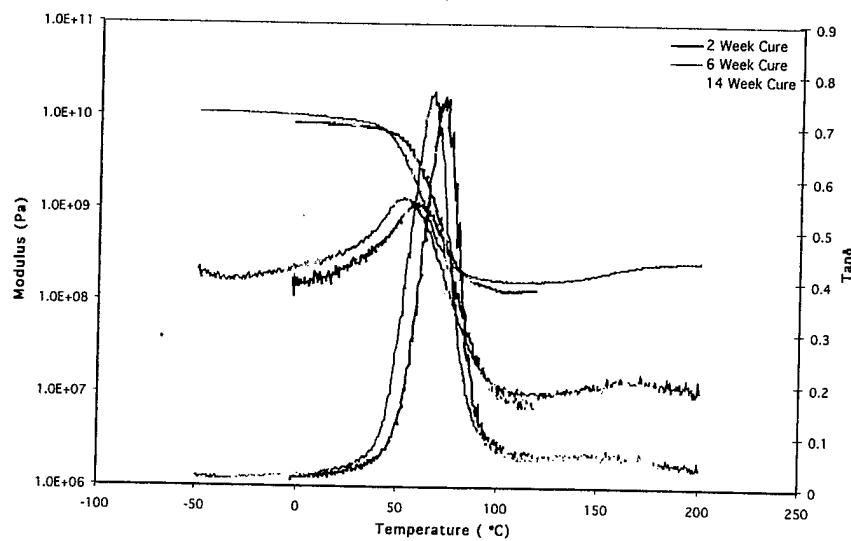

Figure 2: DTR, Mil-C-46168, Free Film
B117 Exposure
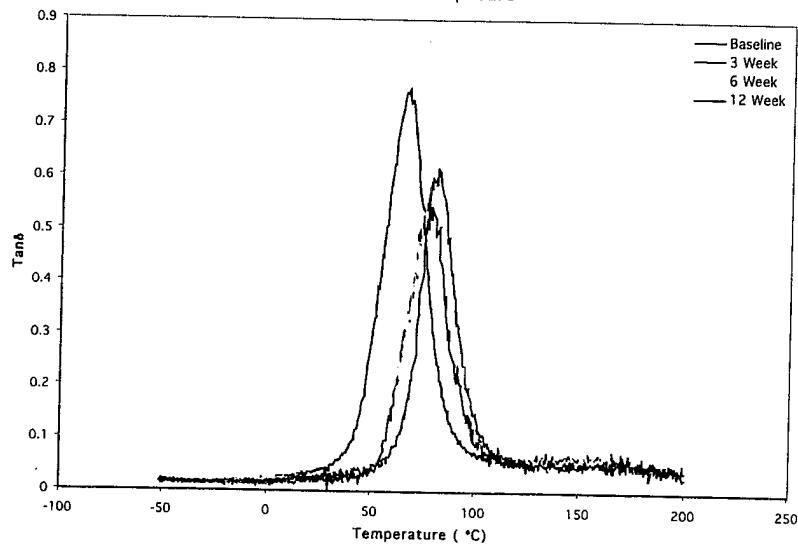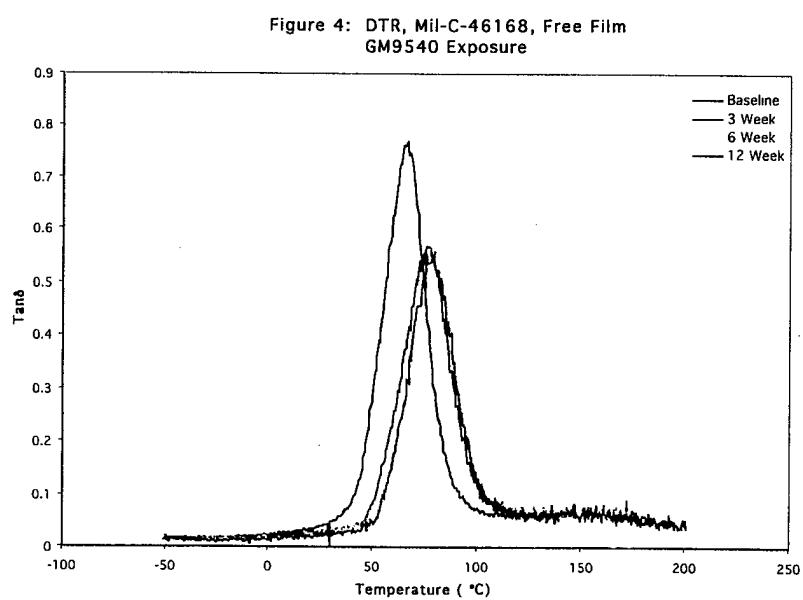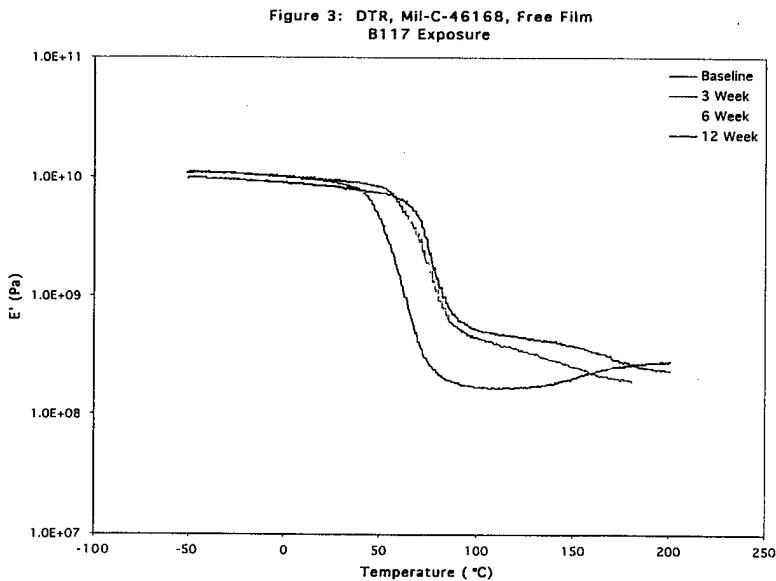
Figure 3: DTR, Mil-C-46168, Free Film
B117 Exposure

Figure 4: DTR, Mil-C-46168, Free Film
GM9540 Exposure

**Figure 5: DTR, Mil-C-46168, Free Film**
GM9540 Exposure
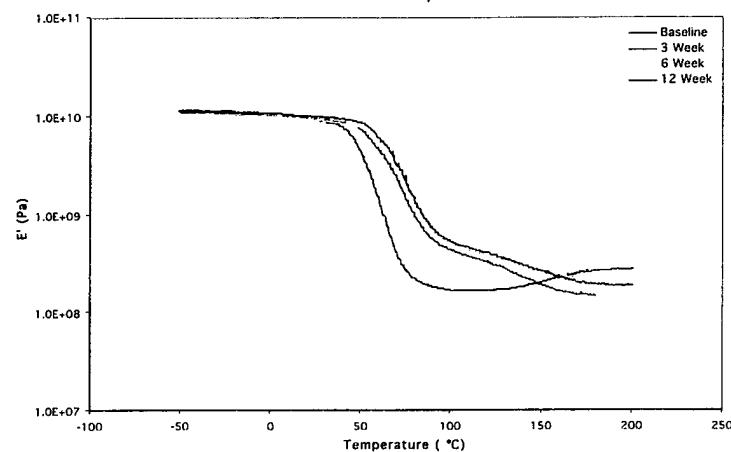
Figure 6: DTR, Mil-C-46168, Free Film
**QUV Exposure**

Figure 7: DTR, Mil-C-46168, Free Film
QUV Exposure

Figure 8: DTR, Mil-C-46168, Free Film
AZ Atlas Exposure
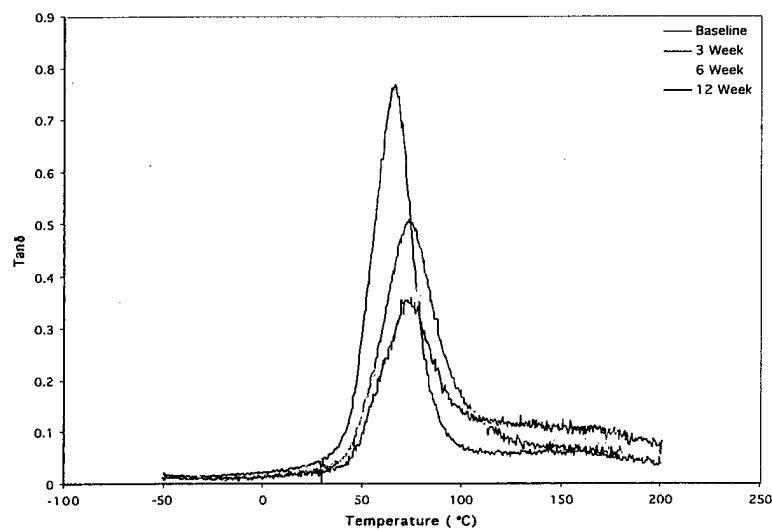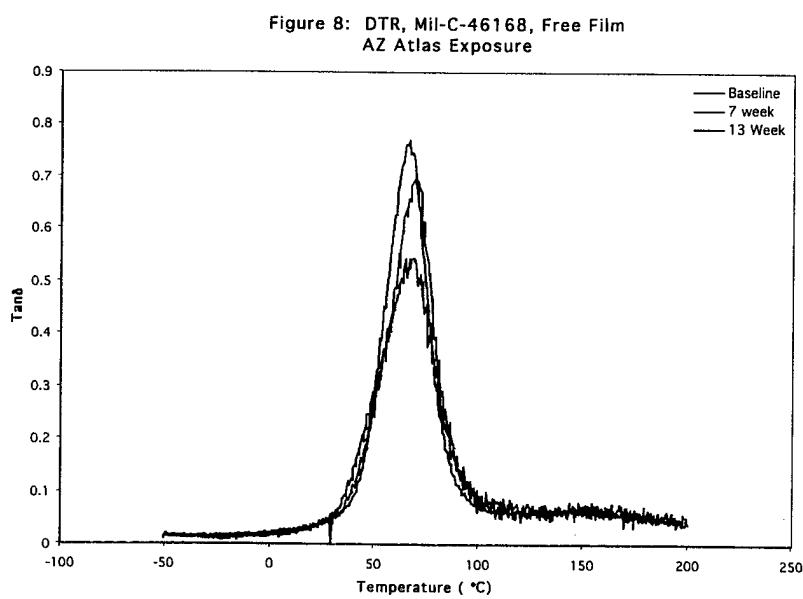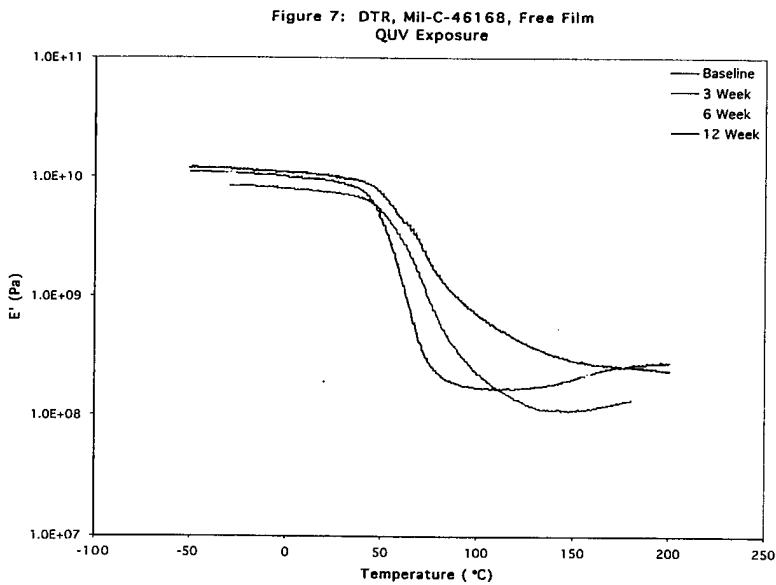
Figure 9: DTR, Mil-C-46168, Free Film
AZ Atlas Exposure

Figure 10: DTR, Mil-C-46168, Free Film
FL Atlas Exposure

**Figure 11: DTR, Mil-C-46168, Free Film
FL Atlas Exposure**
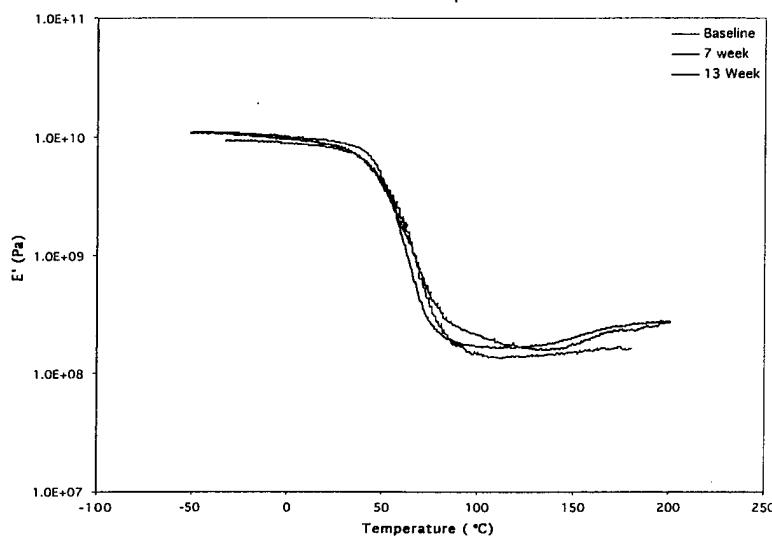
**Figure 12: DTR, Mil-C-46168, Free Film
PA NSWCCD Exposure**
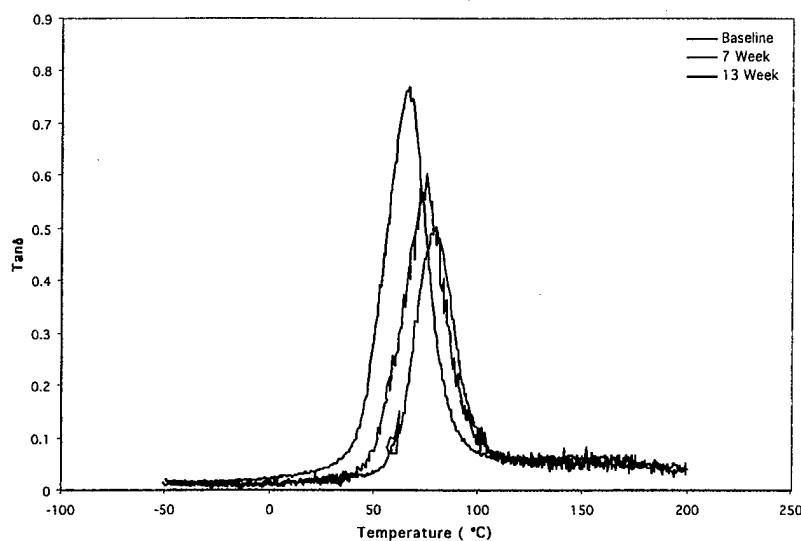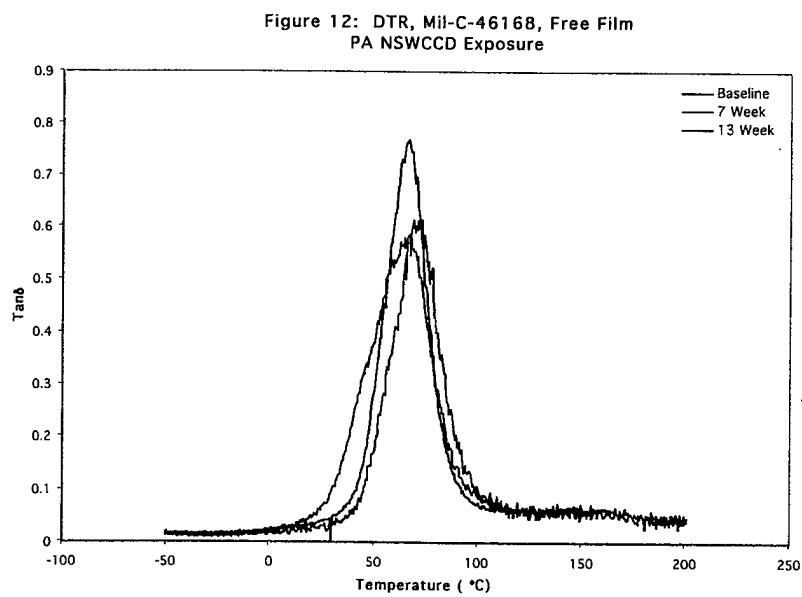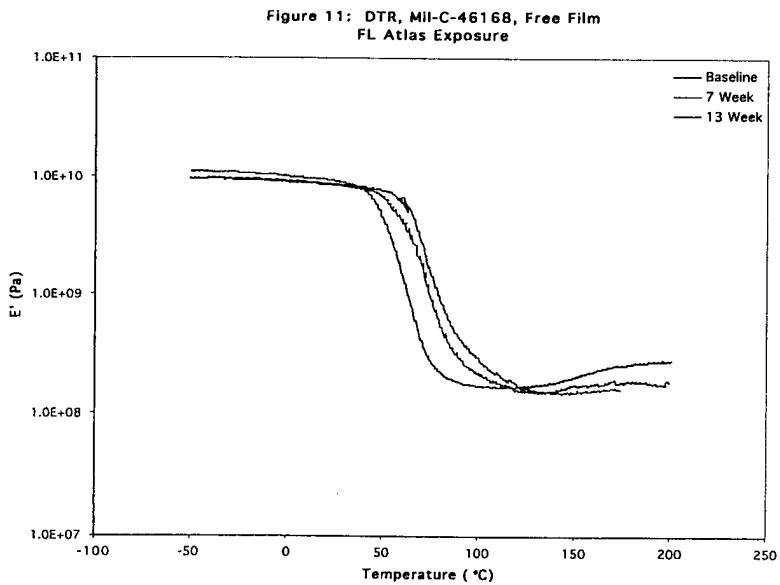
Figure 13: DTR, Mil-C-46168, Free Film
PA NSWCCD Exposure
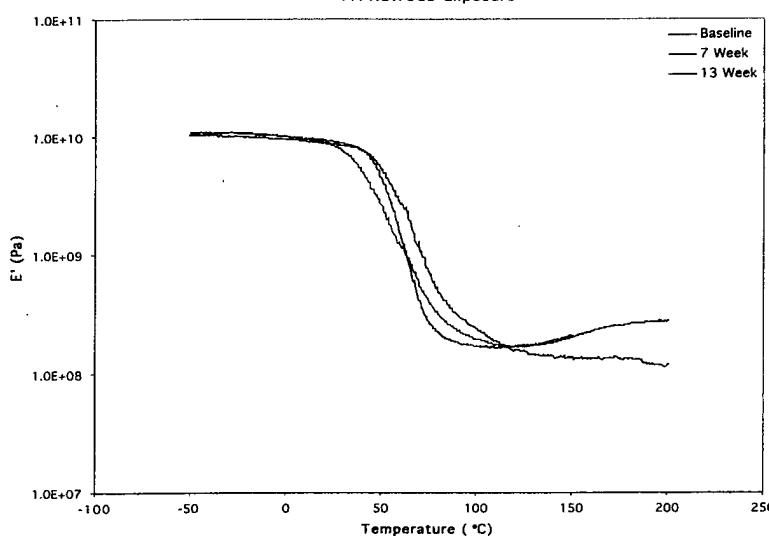
Figure 14: Scatter Plot, Mil-C-46168, Free Film
Effect of Exposure on T_g

Figure 15: Scatter Plot, Mil-C-46168, Free Film
Effect of Exposure on Tanδ_{max}

Figure 16: DTR, Mil-C-64159 TY II, Free Film
Ambient Exposure
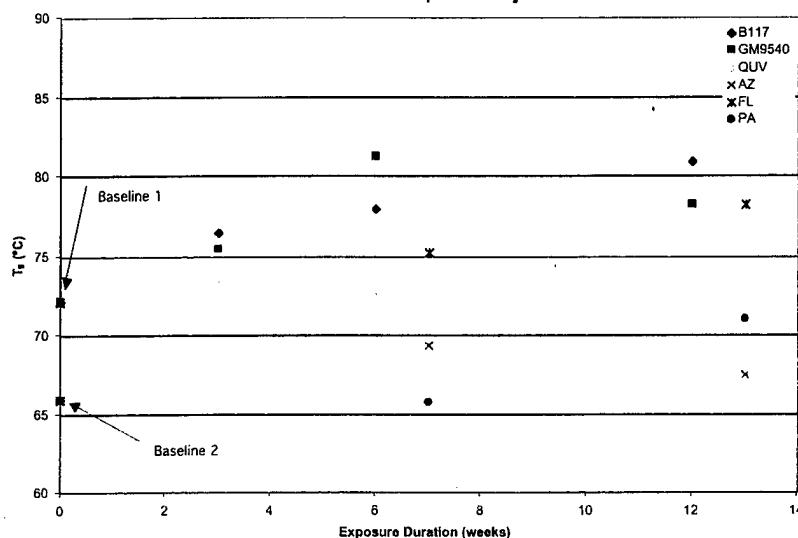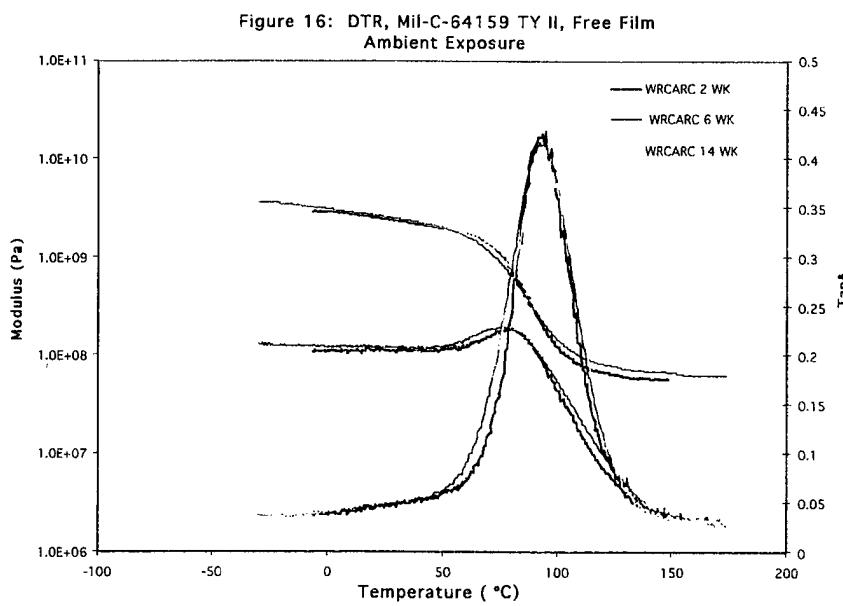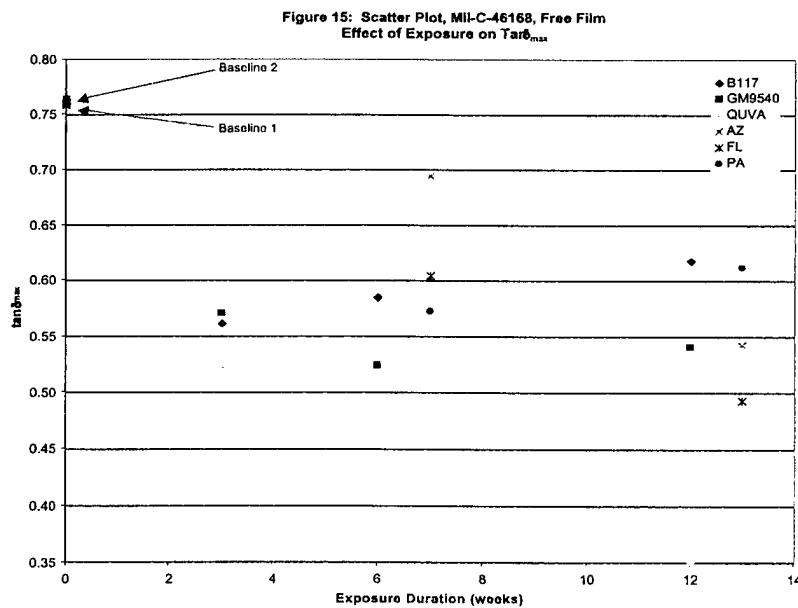
Figure 17: DTR, Mil-C-64159 TY II, Free Film
B117 Exposure
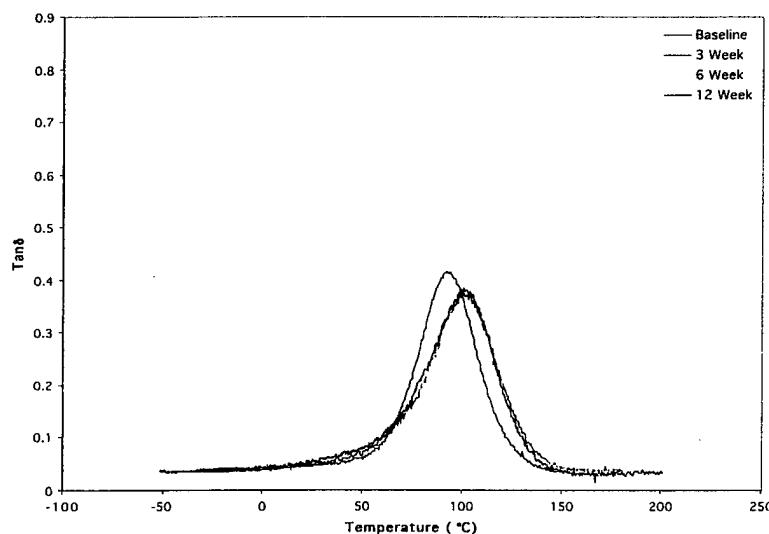
Figure 18: DTR, Mil-C-64159 TY II, Free Film
B117 Exposure
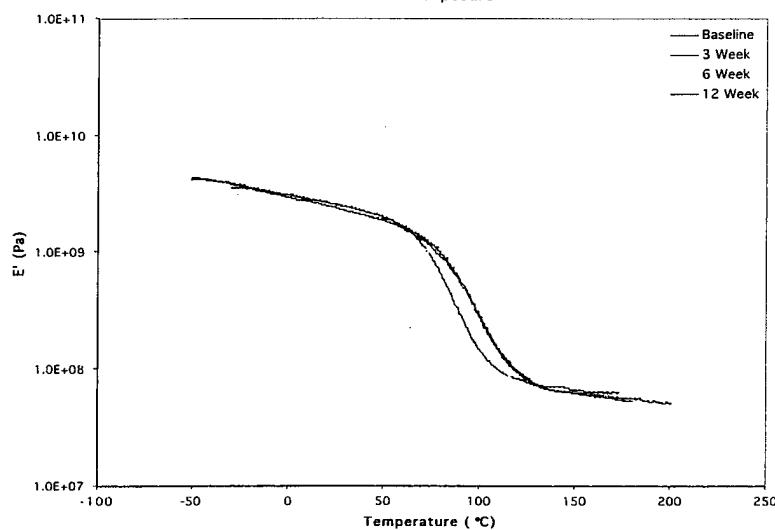
Figure 19: DTR, Mil-C-64159 TY II, Free Film
GM9540 Exposure
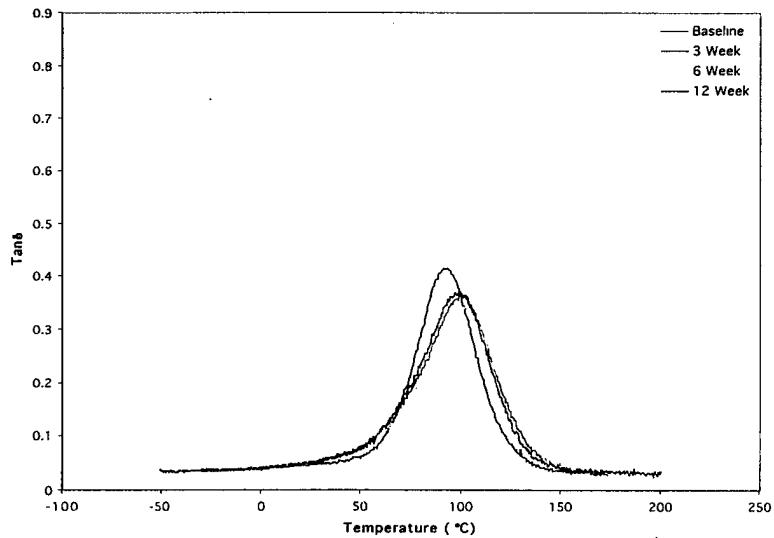
Figure 20: DTR, Mil-C-64159 TY II, Free Film
GM9540 Exposure
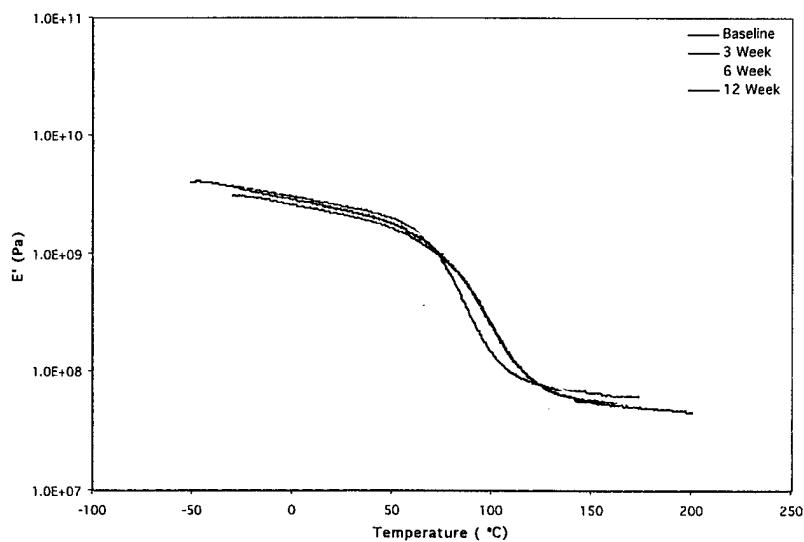
Figure 21: DTR, Mil-C-64159 TY II, Free Film
QUV Exposure
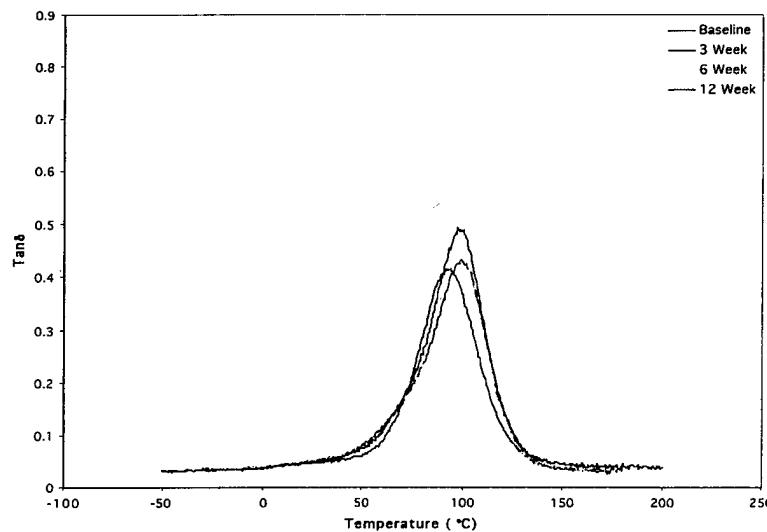
Figure 22: DTR, Mil-C-64159 TY II, Free Film
QUV Exposure
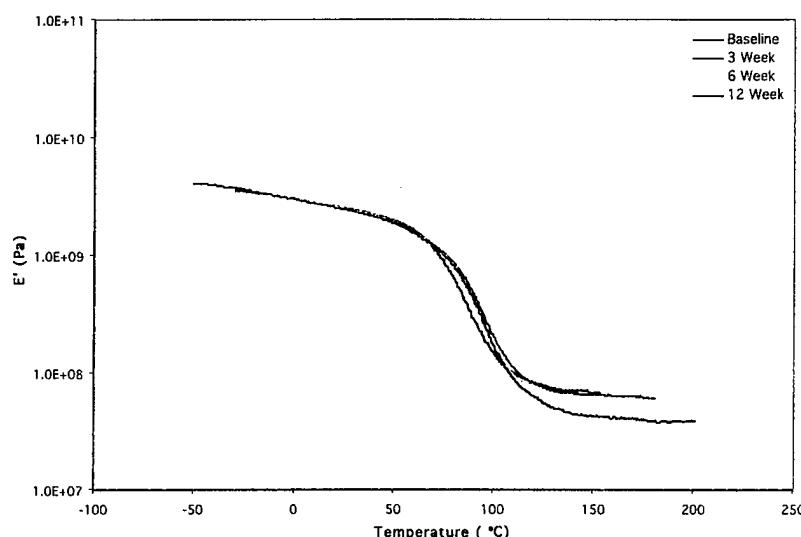
Figure 23: DTR, Mil-C-64159 TY II, Free Film
AZ Atlas Exposure
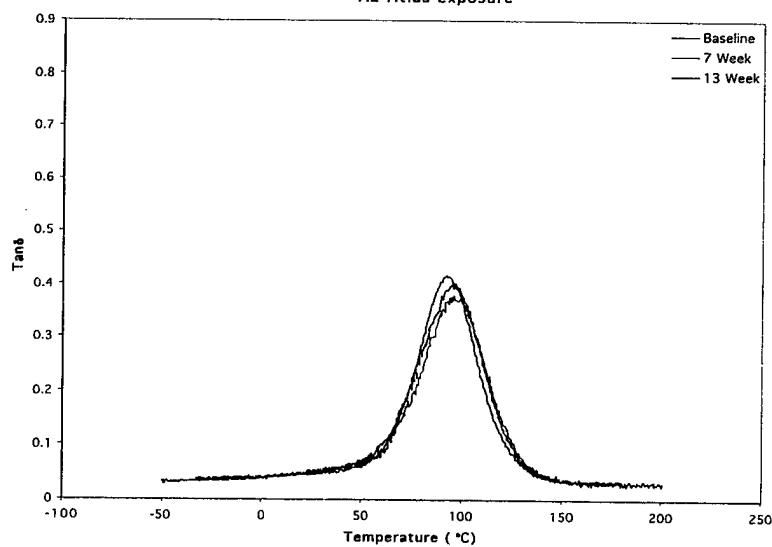
Figure 24: DTR, Mil-C-64159 TY II, Free Film
AZ Atlas Exposure
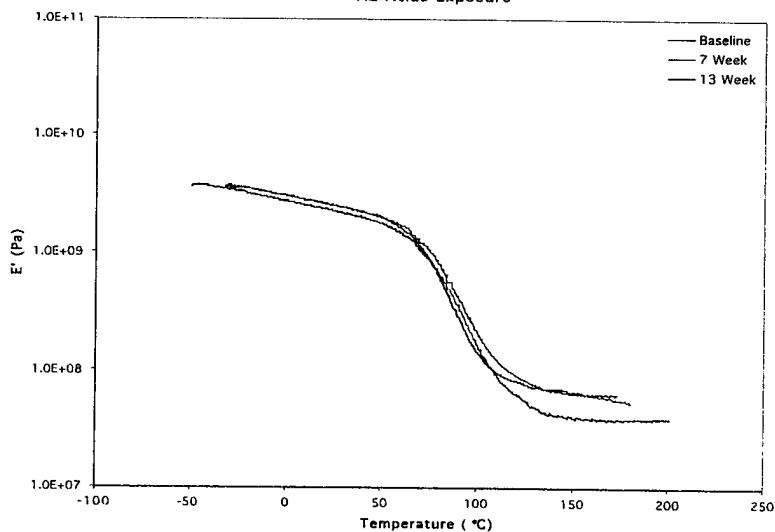
Figure 25: DTR, Mil-C-64159 TY II, Free Film
FL Atlas Exposure
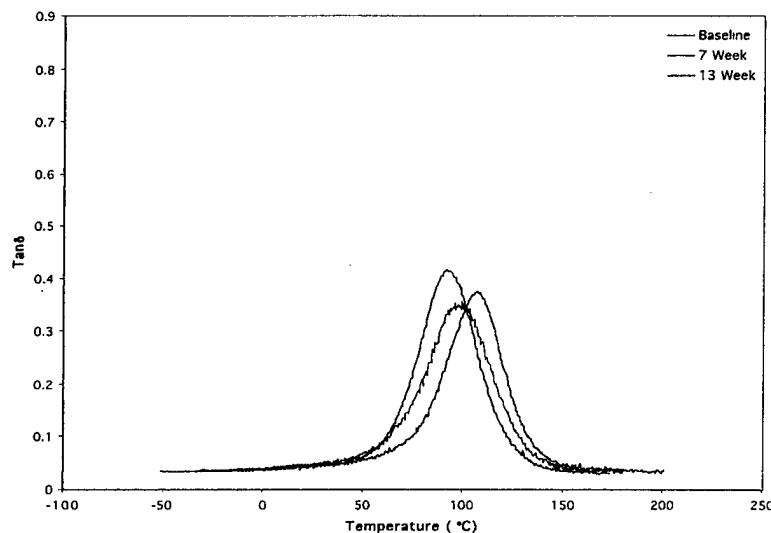
Figure 26: DTR, Mil-C-64159 TY II, Free Film
FL Atlas Exposure
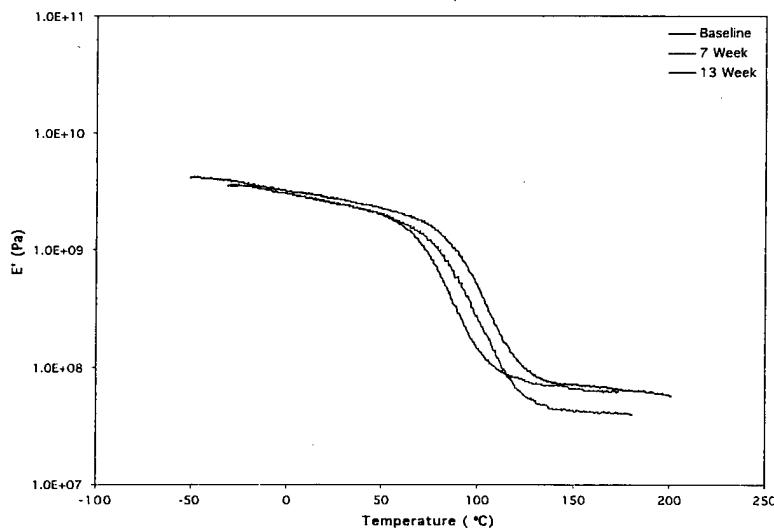
Figure 27: DTR, Mil-C-64159 TY II, Free Film
PA NSWCCD Exposure
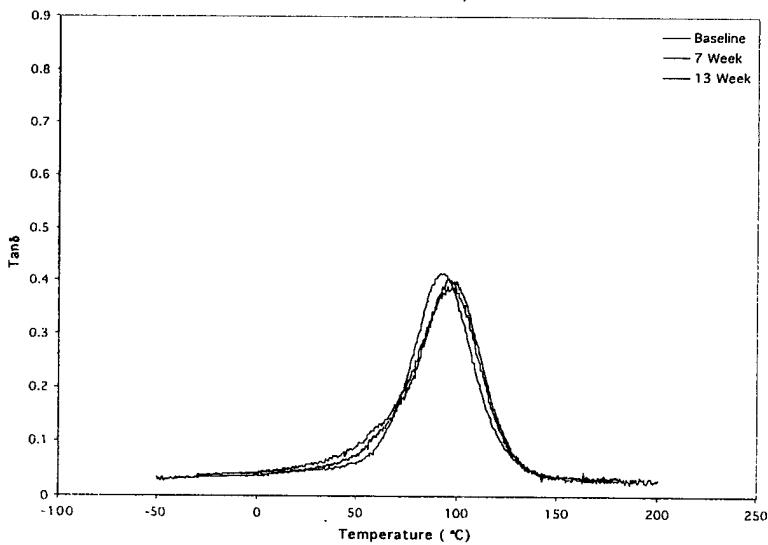
Figure 28: DTR, Mil-C-64159 TY II, Free Film
PA NSWCCD Exposure
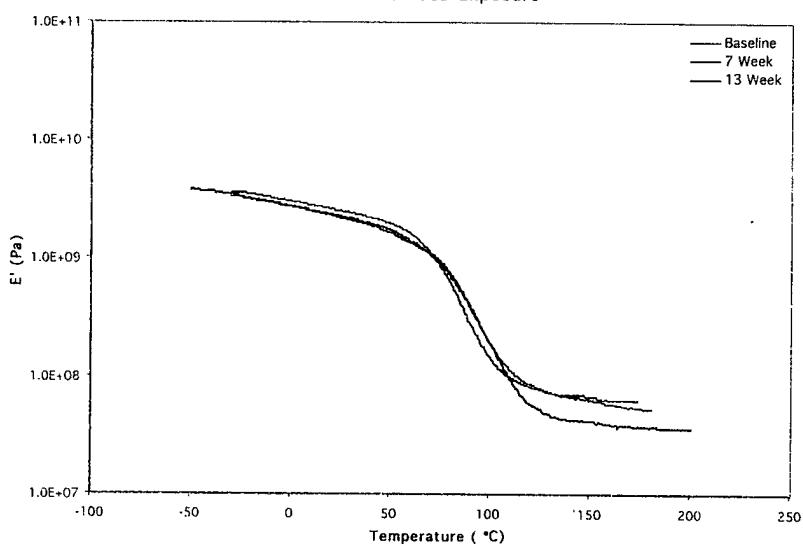
Figure 29: Scatter Plot, Mil-C-64159 TY II, Free Film
**Effect of Exposure on T_g**
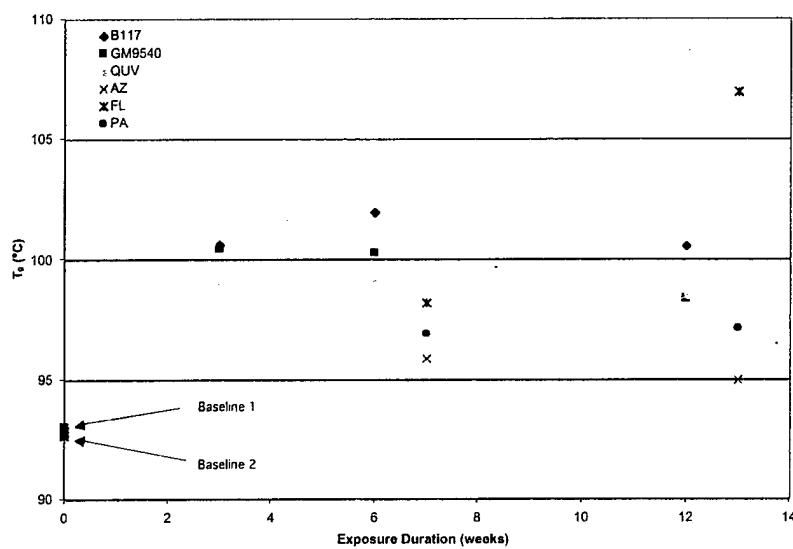
Figure 30: Scatter Plot, Mil-C-64159 TY II, Free Film
Effect of Exposure on $Tan\delta_{max}$
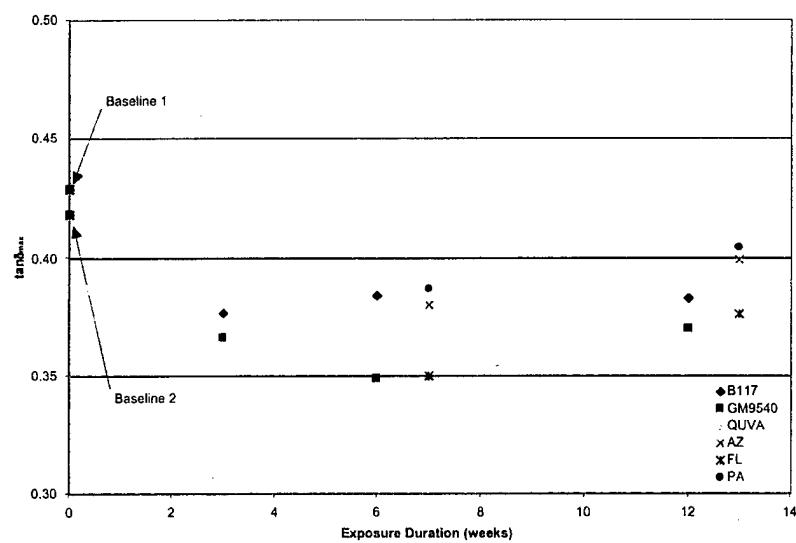
Figure 31: DTR, Mil-C-85285, Free Film
Ambient Exposure
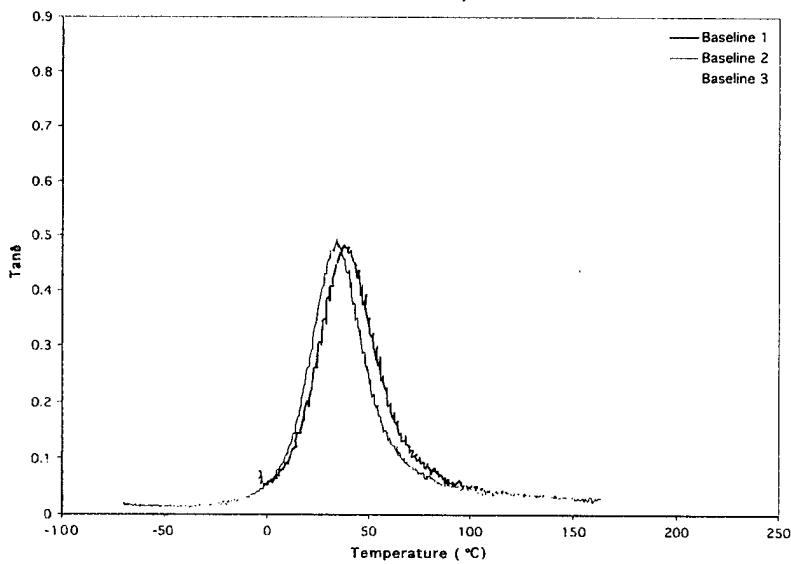
Figure 32: DTR, Mil-C-85285, Free Film
Ambient Exposure
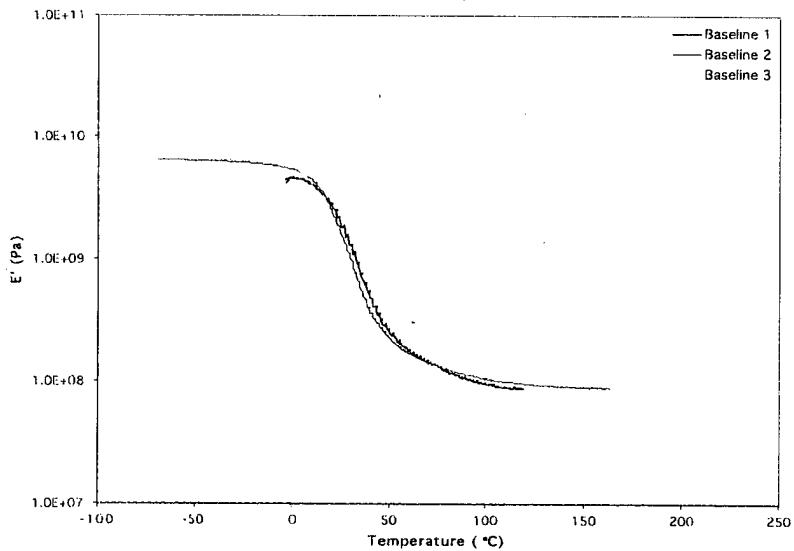
**Figure 33: DTR, Mil-C-85285, Free Film
B117 Exposure**
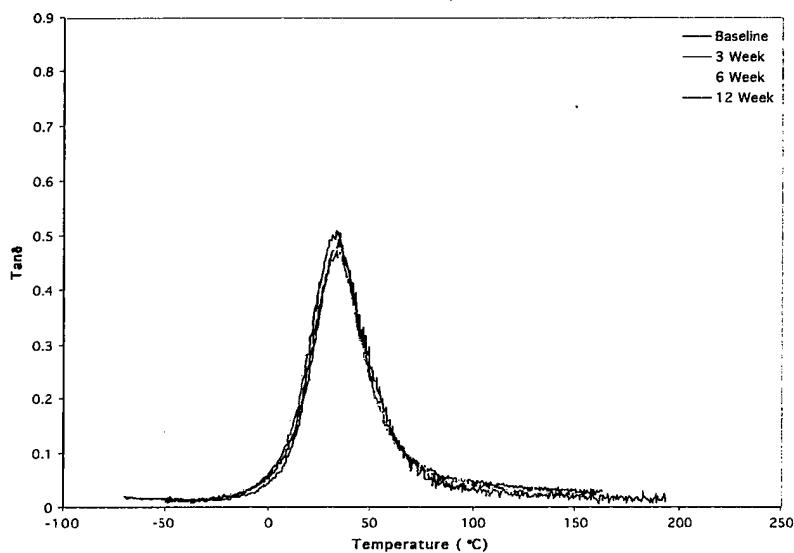
**Figure 34: DTR, Mil-C-85285, Free Film
B117 Exposure**
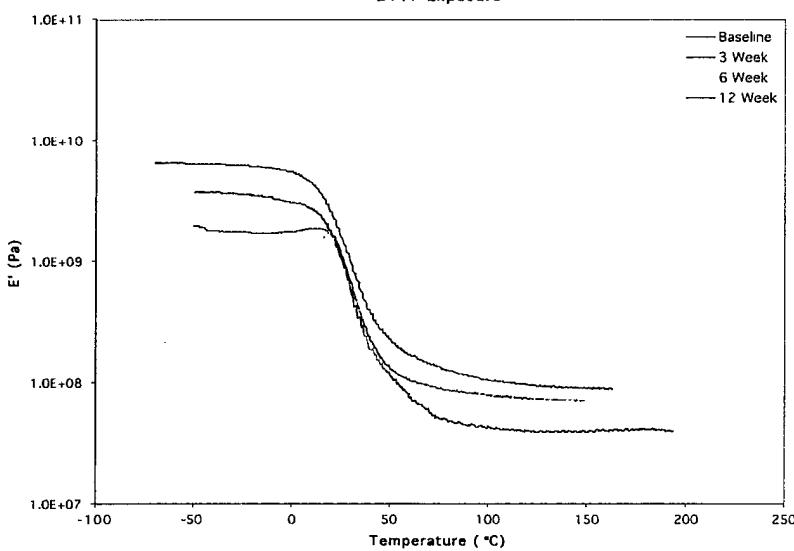
Figure 35: DTR, Mil-C-85285, Free Film
GM9540 Exposure
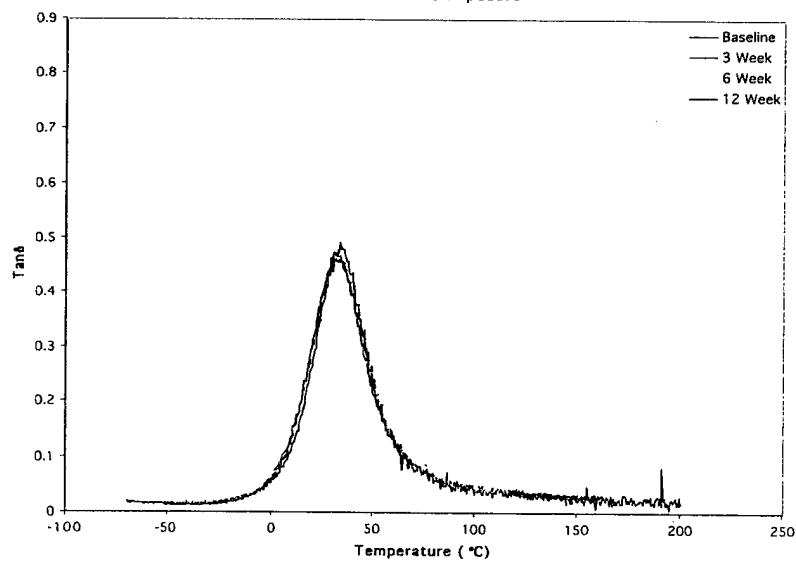
Figure 36: DTR, Mil-C-85285, Free Film
GM9540 Exposure
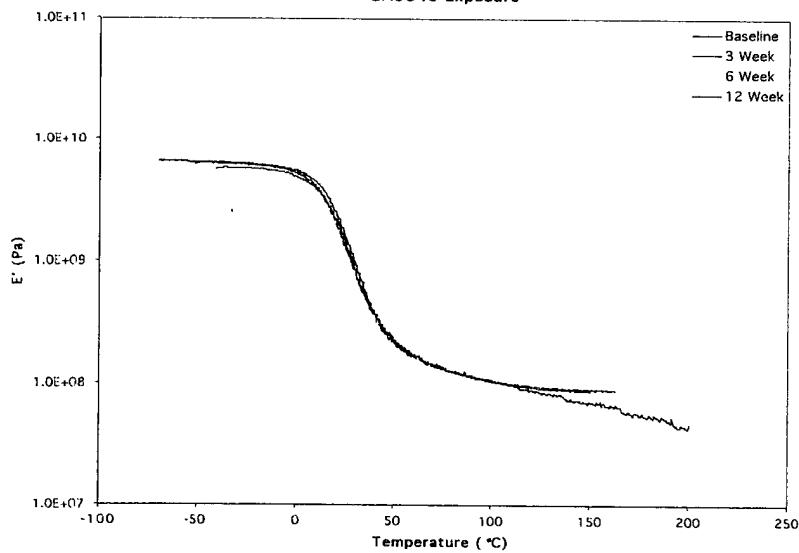
Figure 37: DTR, Mil-C-85285, Free Film
QUV Exposure
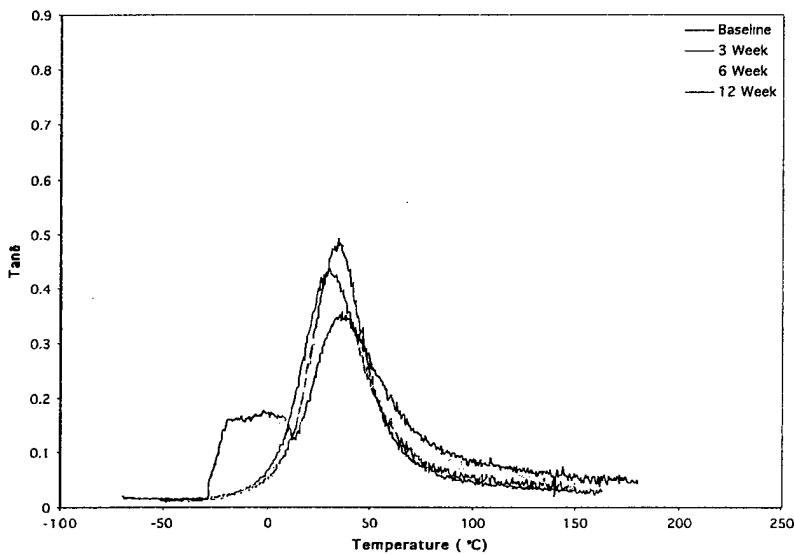
Figure 38: DTR, Mil-C-85285, Free Film
QUV Exposure
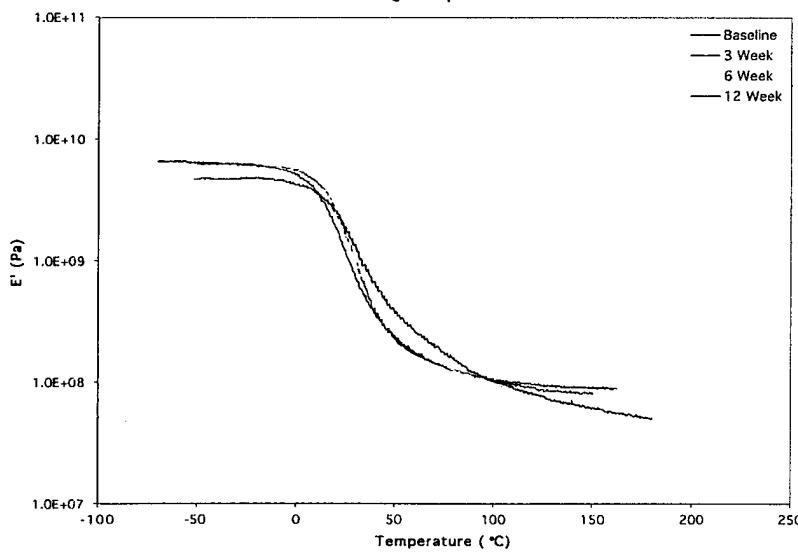
**Figure 39: DTR, Mil-C-85285, Free Film
AZ Atlas Exposure**
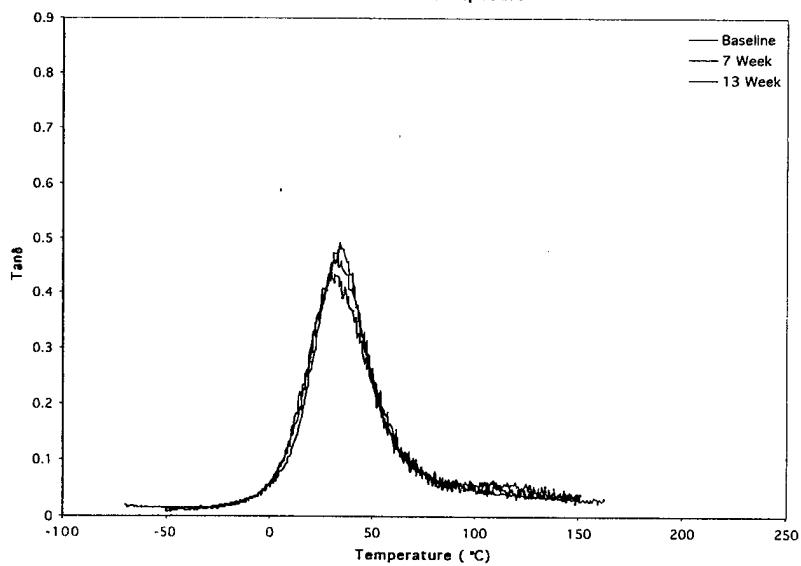
**Figure 40: DTR, Mil-C-85285, Free Film
AZ Atlas Exposure**
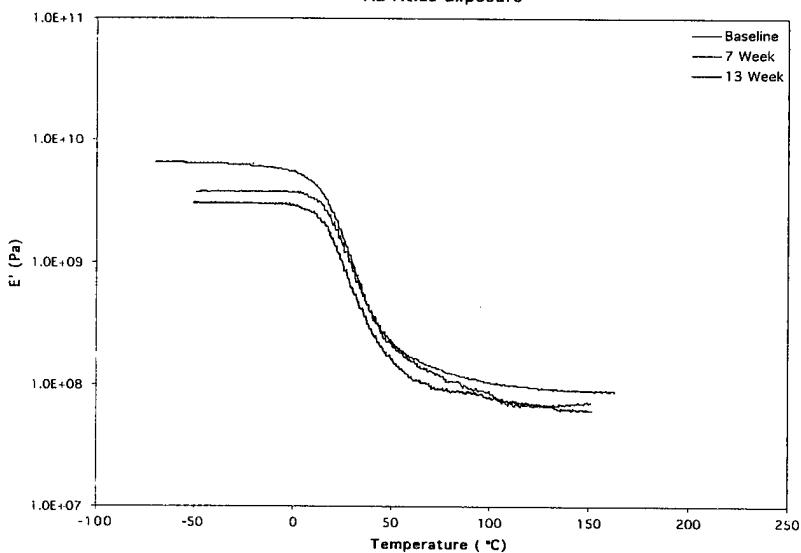
Figure 41: DTR, Mil-C-85285, Free Film
FL Atlas Exposure
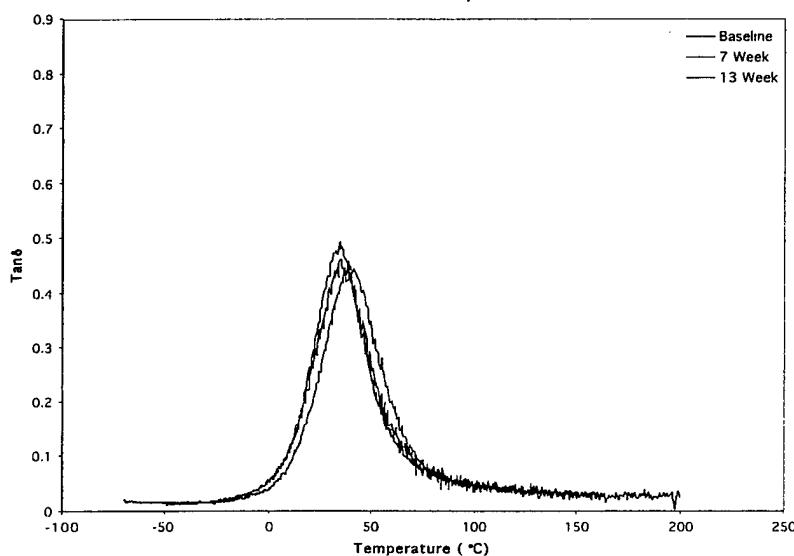
Figure 42: DTR, Mil-C-85285, Free Film
FL Atlas Exposure

34
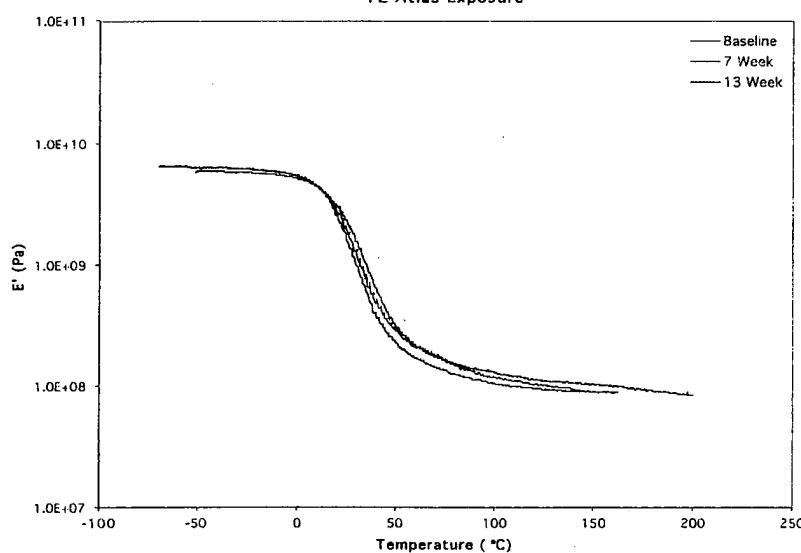
Figure 43: DTR, Mil-C-85285, Free Film
PA NSWCCD Exposure
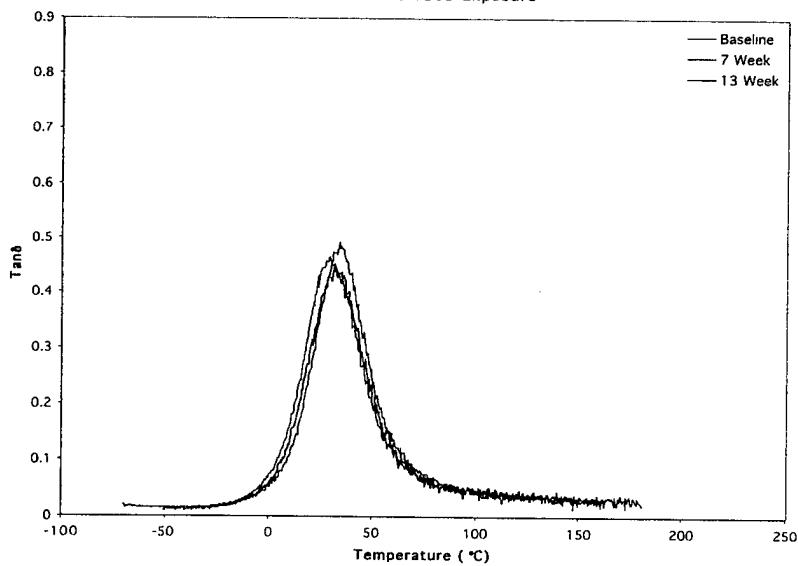
Figure 44: DTR, Mil-C-85285, Free Film
PA NSWCCD Exposure
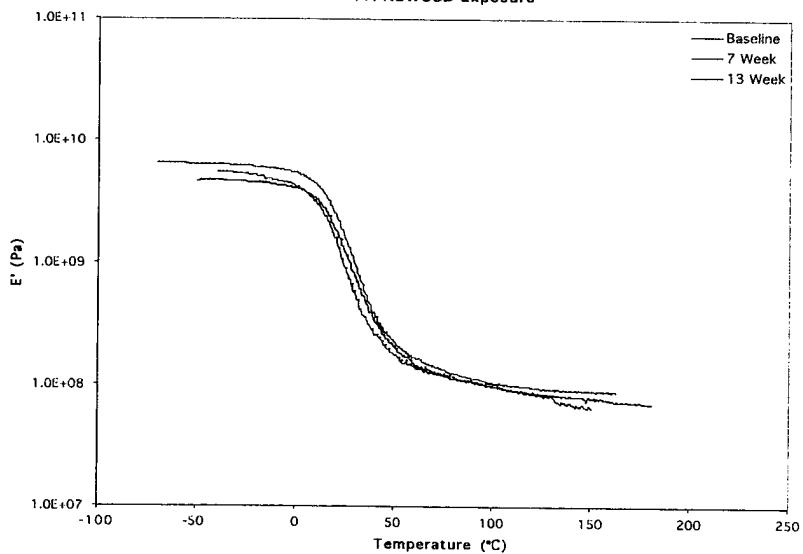
Figure 45: Scatter Plot, Mil-C-85285, Free Film
Effect of Exposure on T_g
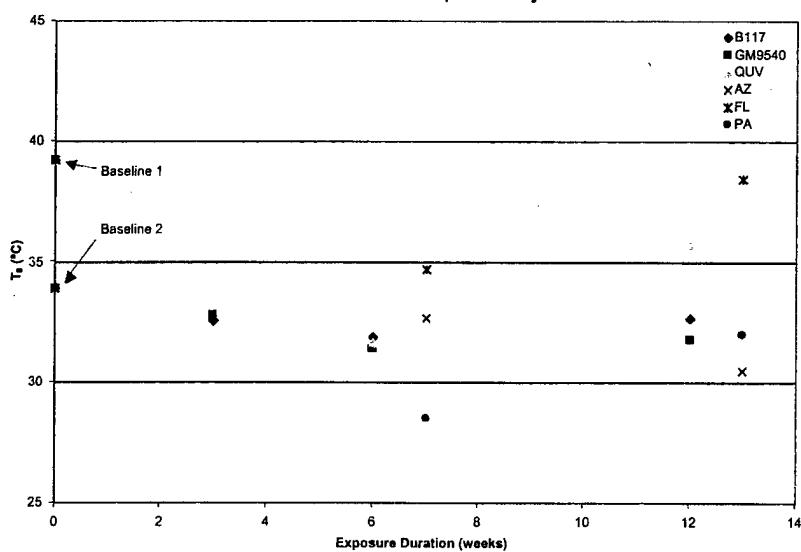
Figure 46: Scatter Plot, Mil-C-85285, Free Film
Effect of Exposure on $Tan\delta_{max}$
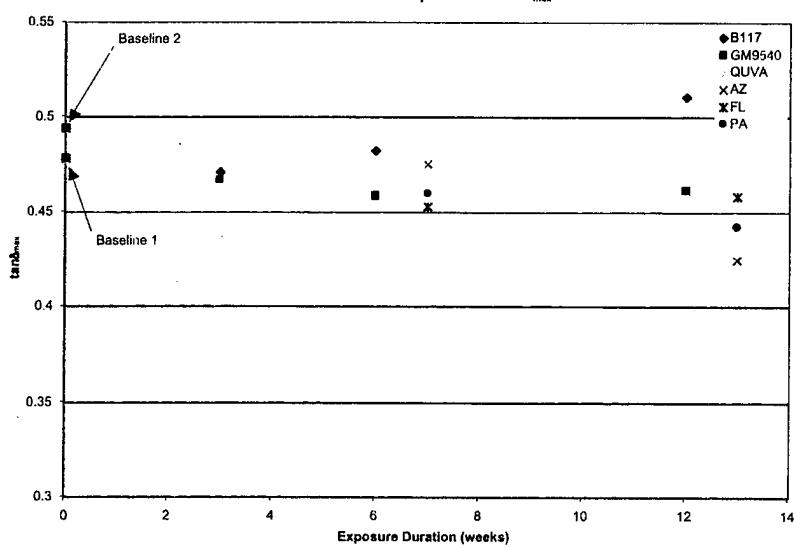
Figure 47: DTR, ZVOC TC, Free Film
Ambient Exposure
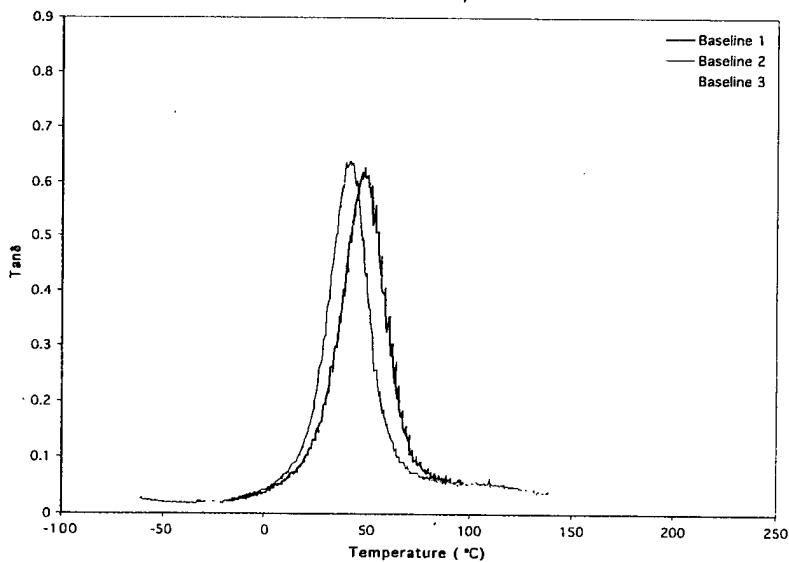
Figure 48: DTR, ZVOC TC, Free Film
Ambient Exposure
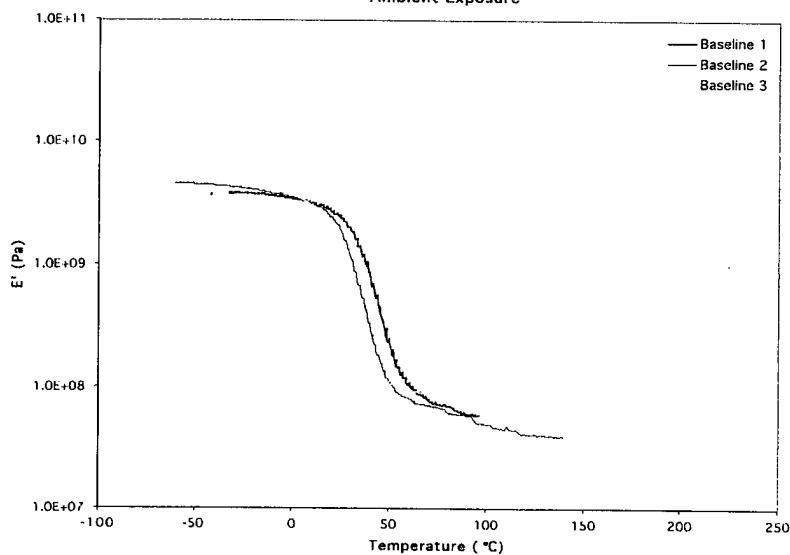
Figure 49: DTR, ZVOC TC, Free Film
B117 Exposure
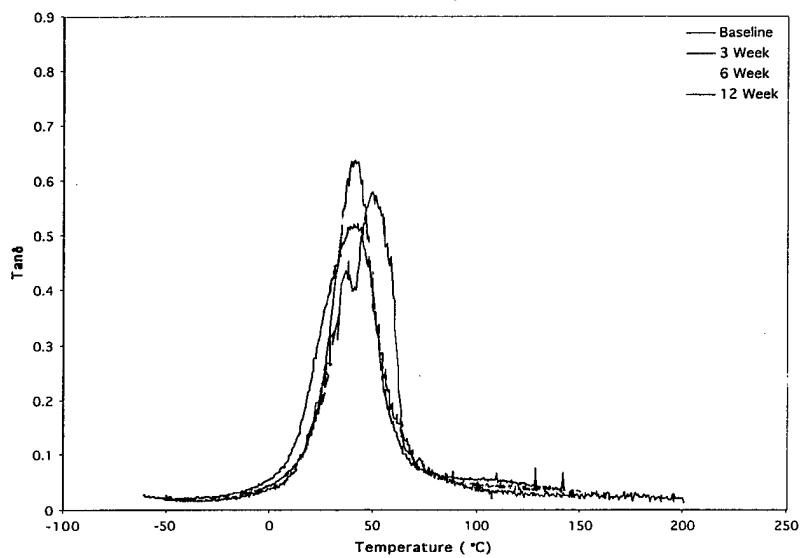
Figure 50: DTR, ZVOC TC, Free Film
B117 Exposure

Figure 51: DTR, ZVOC TC, Free Film
GM9540 Exposure

Figure 52: DTR, ZVOC TC, Free Film
GM9540 Exposure

Figure 53: DTR, ZVOC TC, Free Film
QUV Exposure

Figure 54: DTR, ZVOC TC, Free Film
QUV Exposure
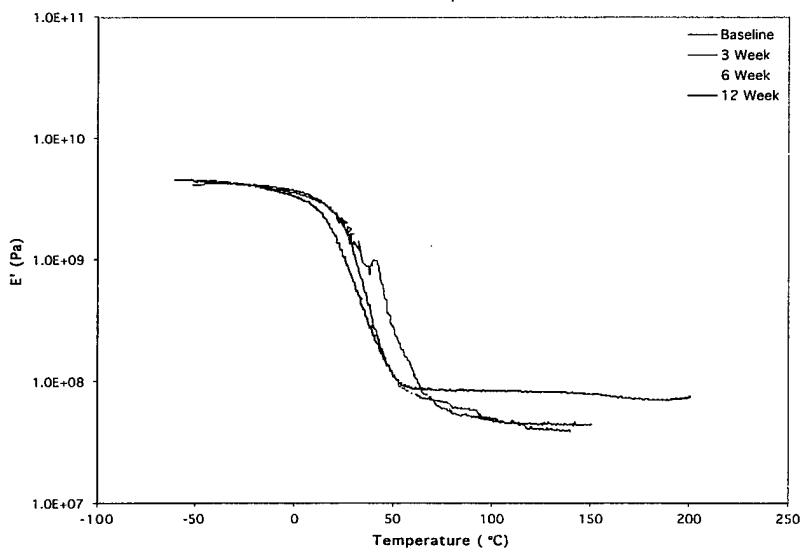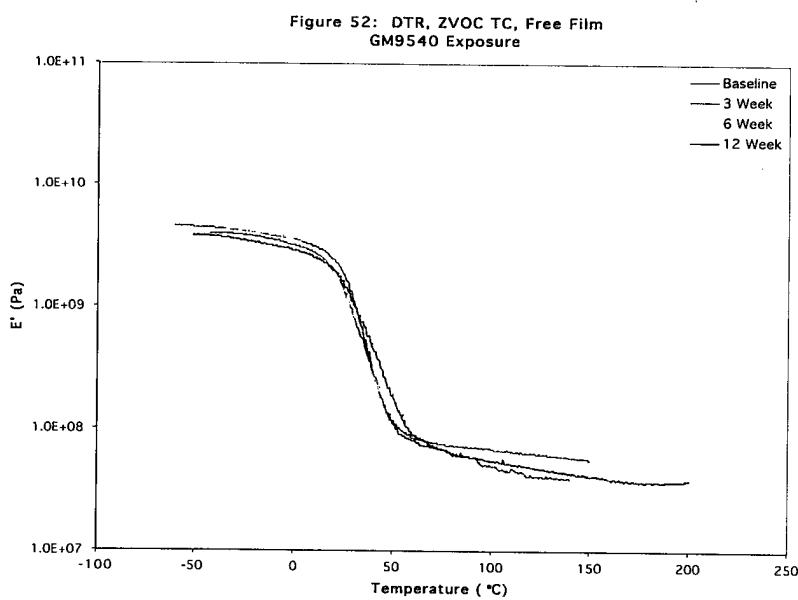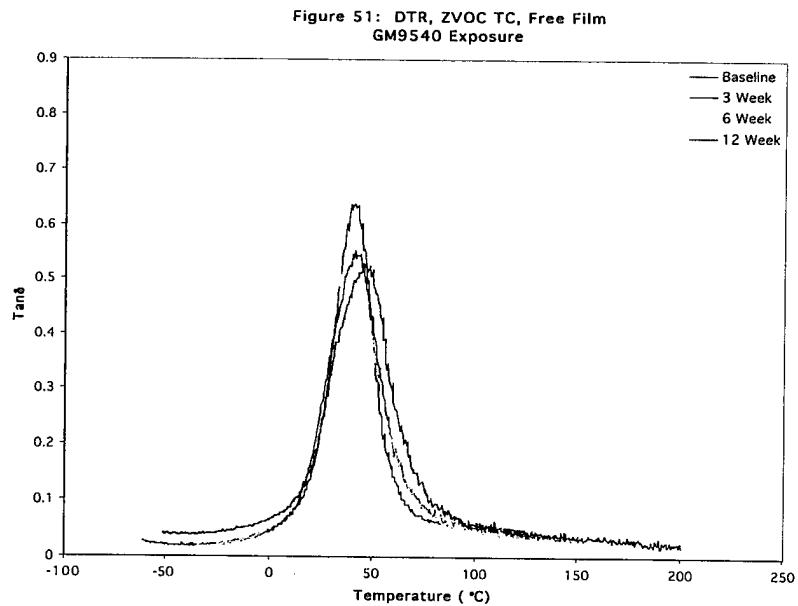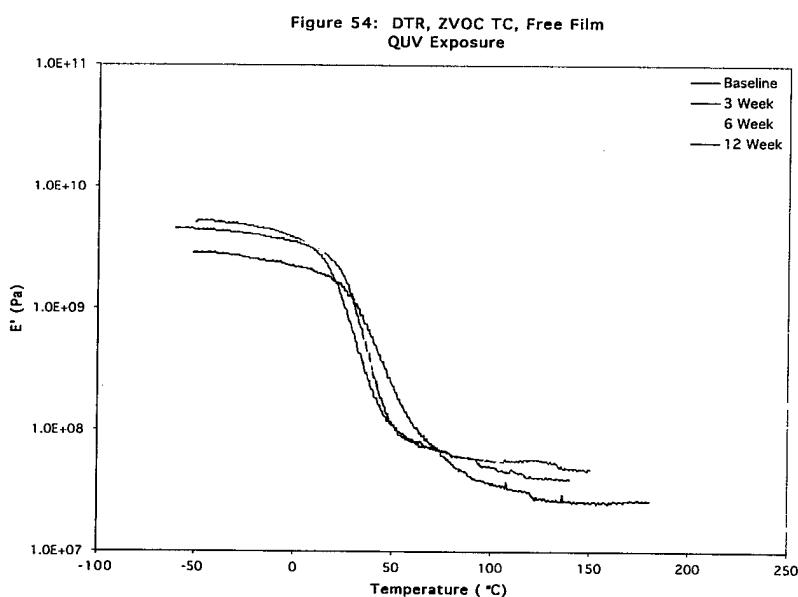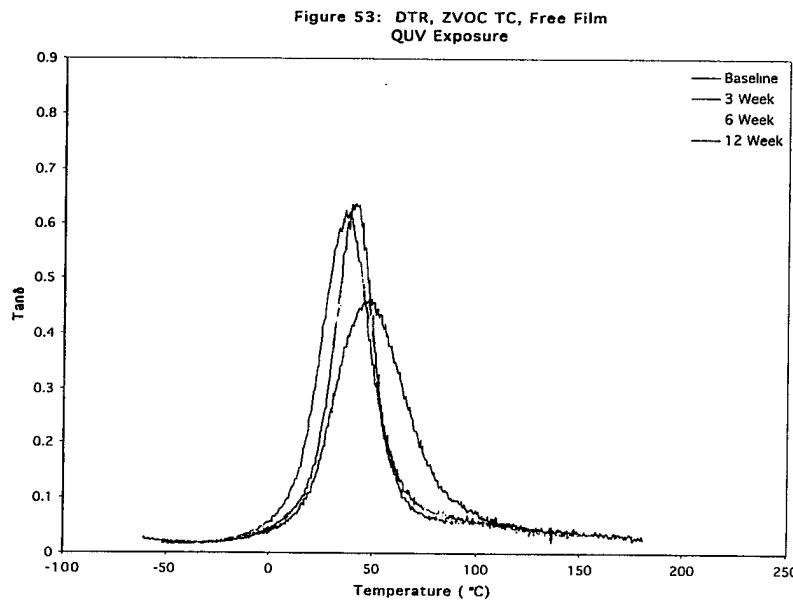
Figure 55: DTR, ZVOC TC, Free Film
AZ Atlas Exposure
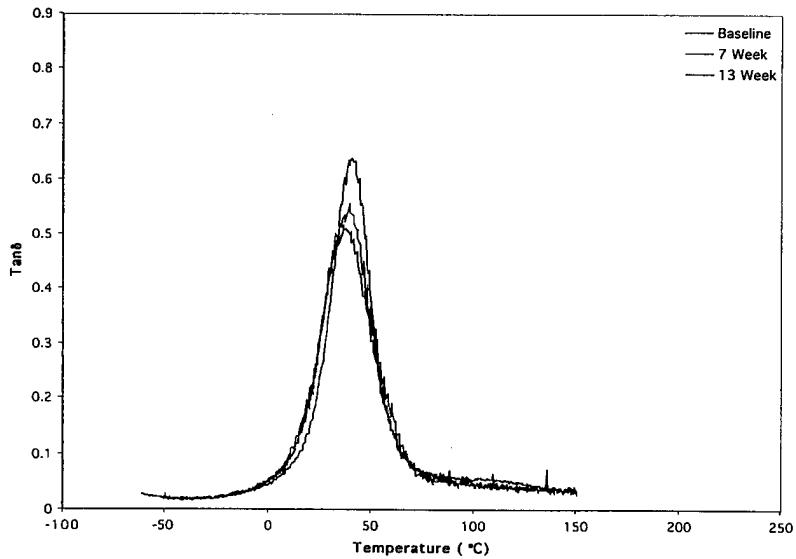
Figure 56: DTR, ZVOC TC, Free Film
AZ Atlas Exposure
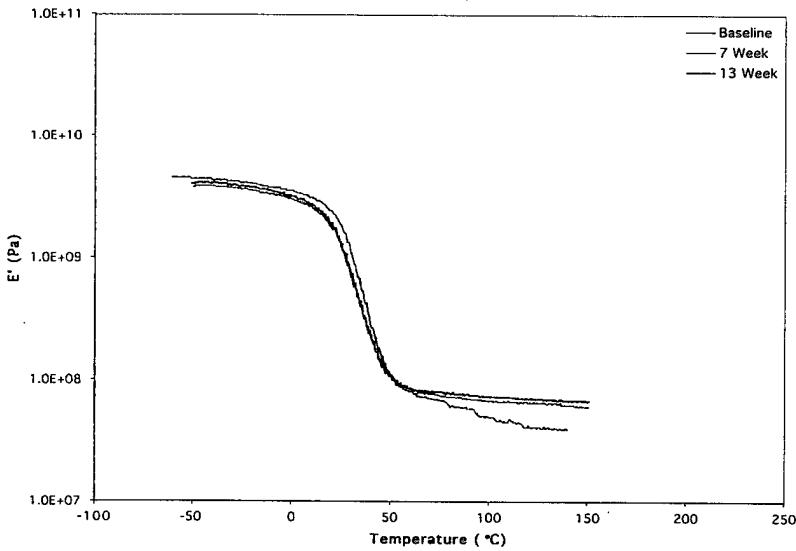
Figure 57: DTR, ZVOC TC, Free Film
FL Atlas Exposure
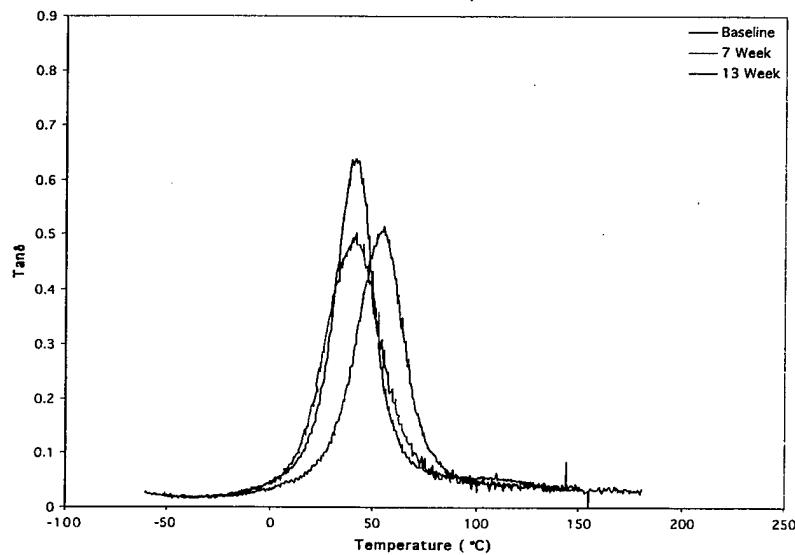
Figure 58: DTR, ZVOC TC, Free Film
FL Atlas Exposure
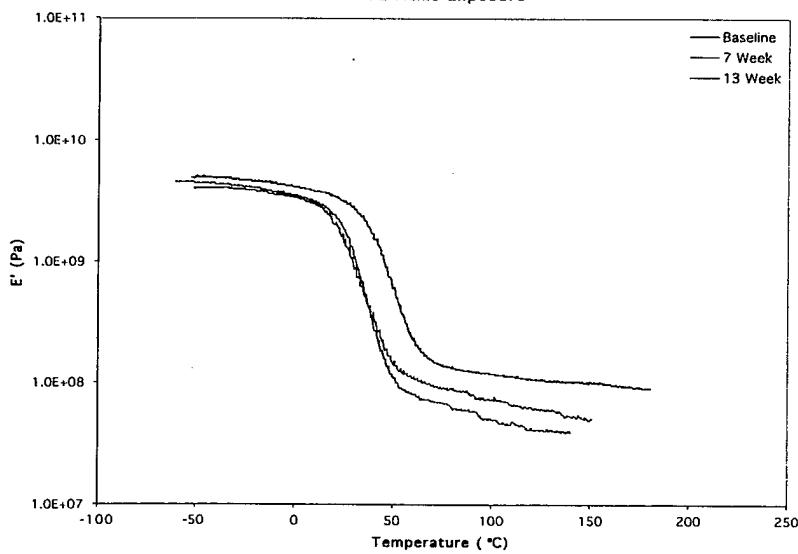
Figure 59: DTR, ZVOC TC, Free Film
PA NSWCCD Exposure
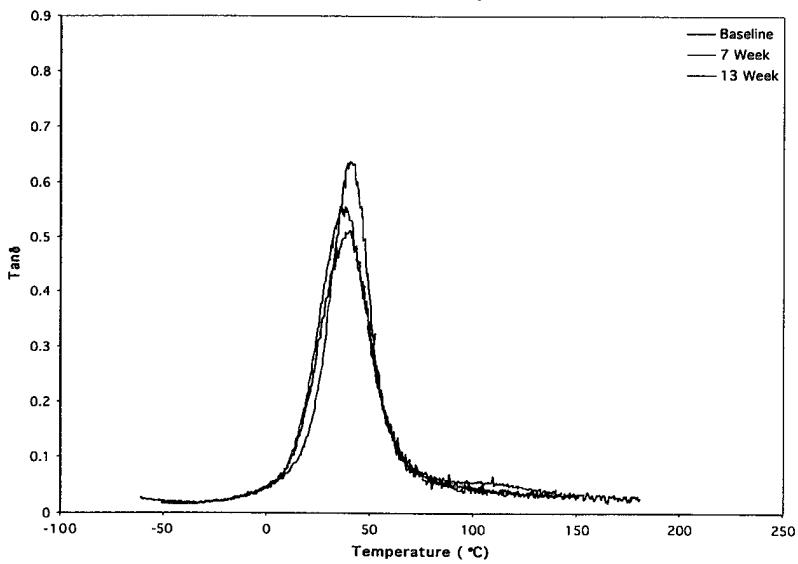
Figure 60: DTR, ZVOC TC, Free Film
PA NSWCCD Exposure
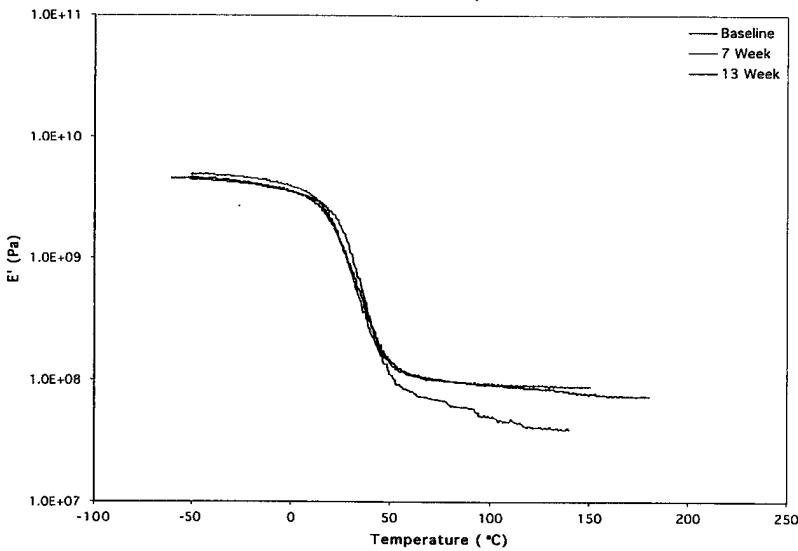
Figure 61: Scatter Plot, ZVOC TC, Free Film
Effect of Exposure on T_g
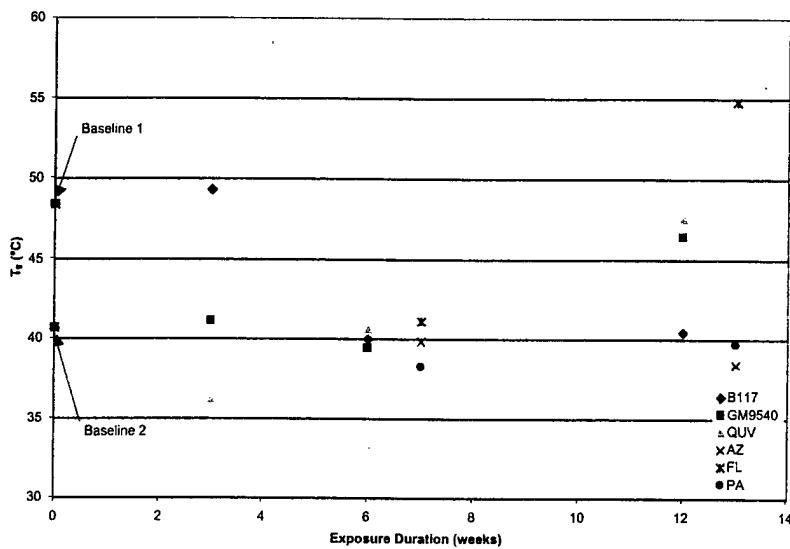
Figure 62: Scatter Plot, ZVOC TC, Free Film
Effect of Exposure on $Tan\delta_{max}$
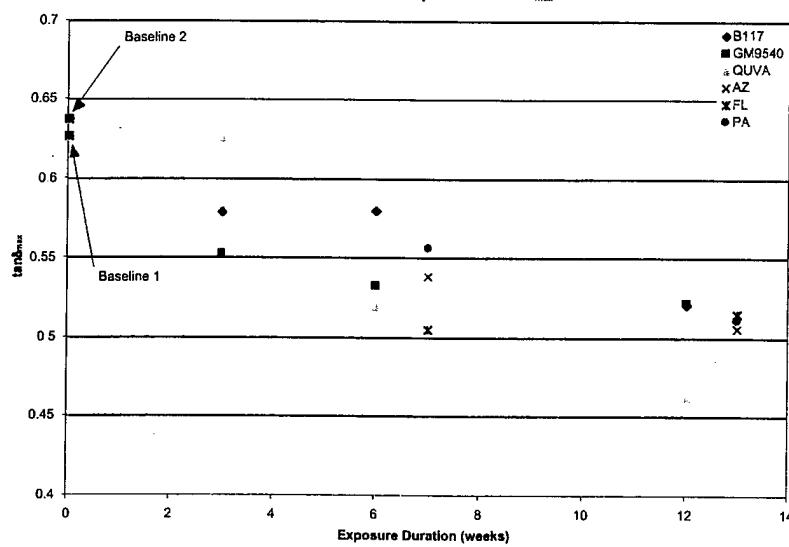
Figure 63: DTR, MIL-C-46168, Mesh
Ambient Exposure
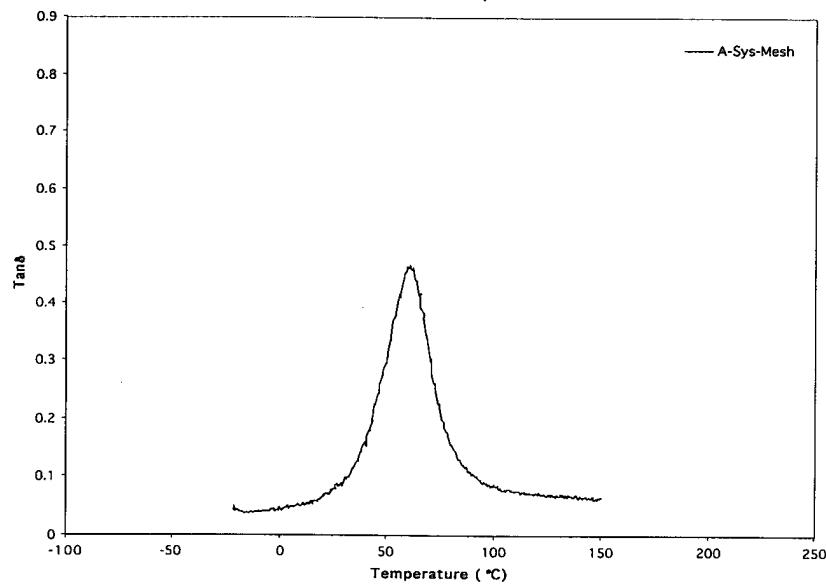
Figure 64: DTR, MIL-C-64159 TY II
Substrate Effect (Ambient Exposure)
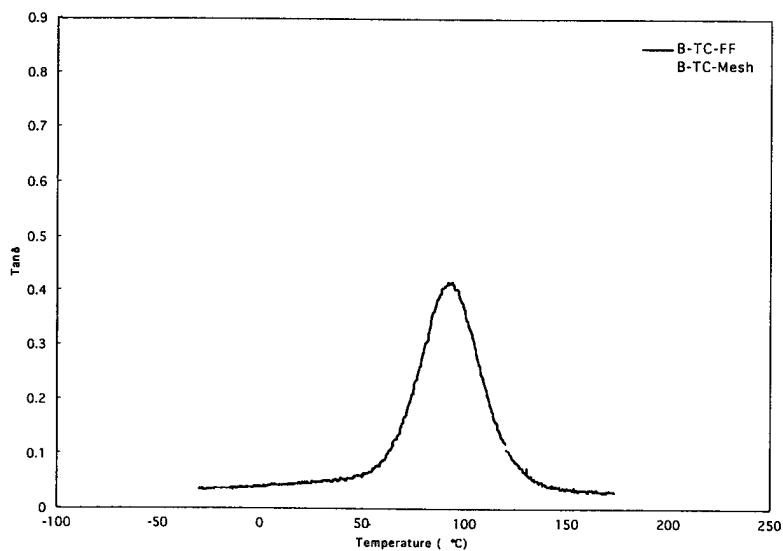
Figure 65: DTR, MIL-C-64159 TY II, Mesh
Ambient Exposure
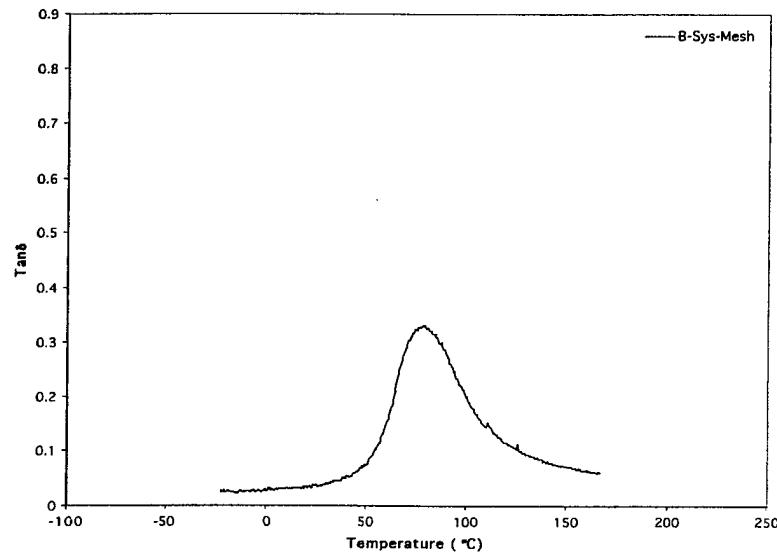
Figure 66: DTR, MIL-C-85285, Mesh
Ambient Exposure

Figure 67: DTR, ZVOC TC, Mesh
Ambient Exposure

Figure 68: Time Sweep, MIL-C-46168, Mesh
Day 1 - 4
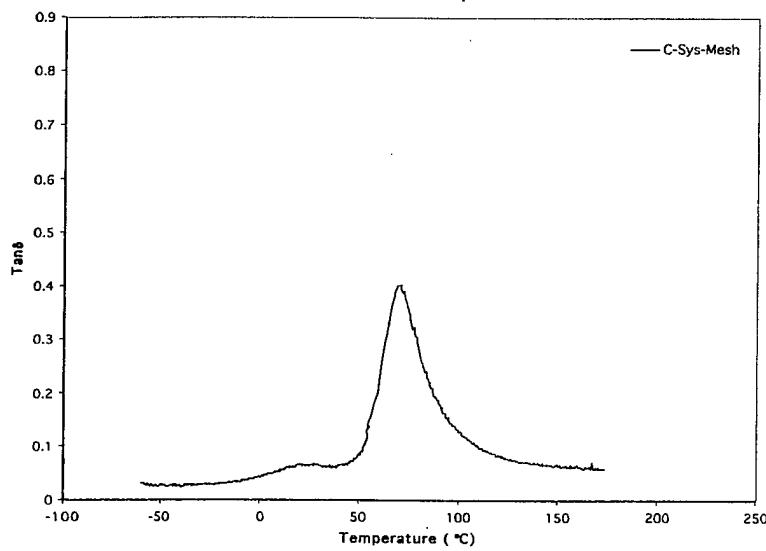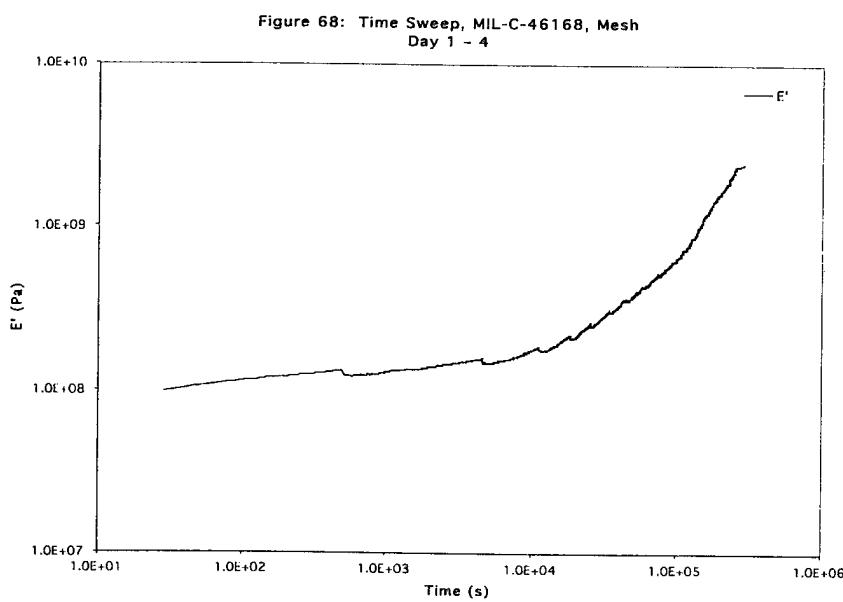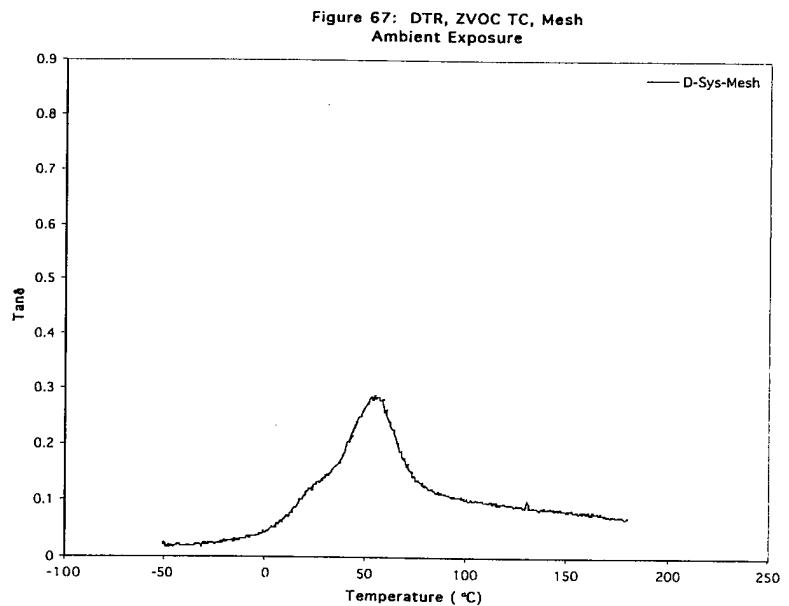
Figure 69: Time Sweep, MIL-C-46168, Mesh
Day 4 – 5
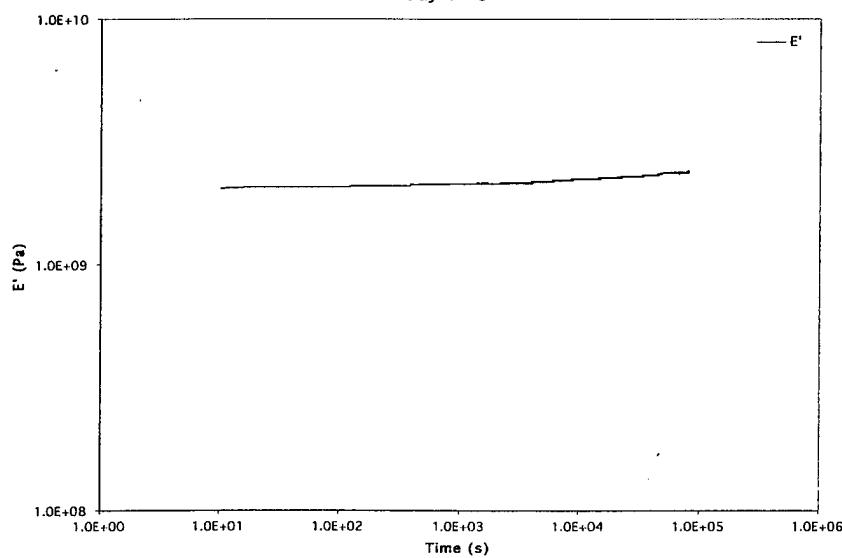
Figure 70: Time Sweep, MIL-C-46168, Mesh
**Day 5 – 6**
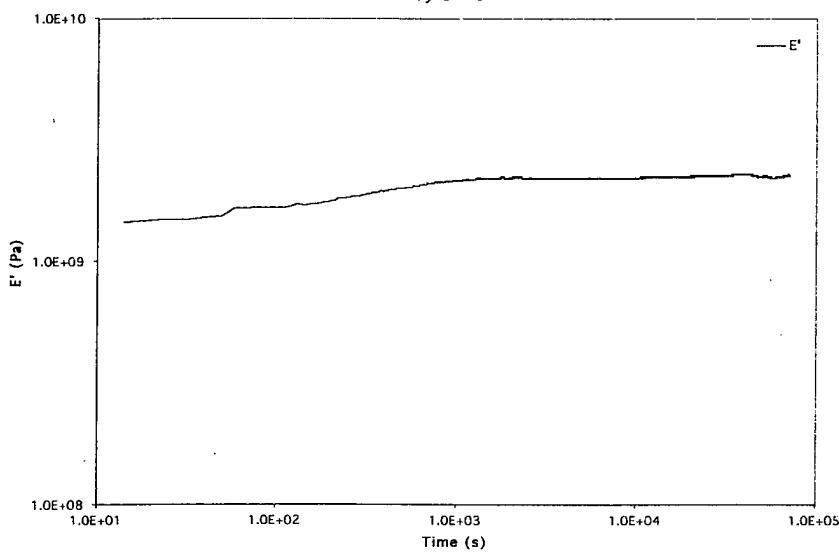
Figure 71: Scatter Plot, MIL-C-46168, Free Film
Effect of Exposure on Density
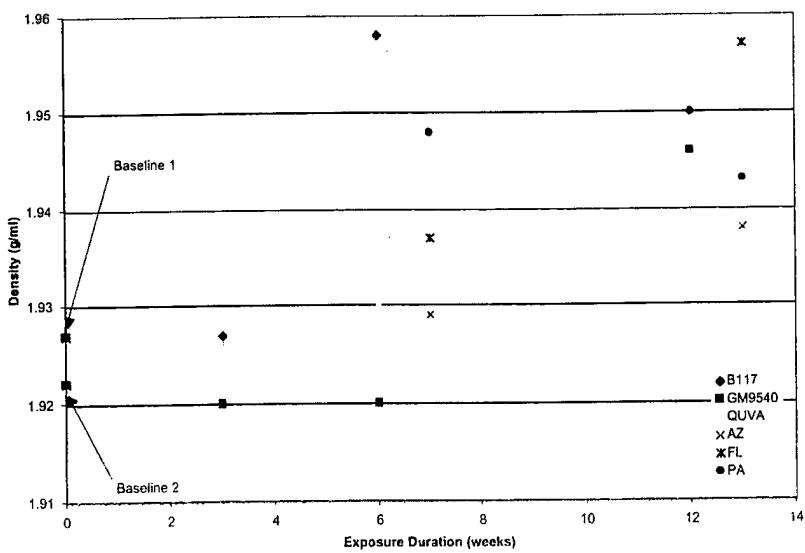
Figure 72: Scatter Plot, MIL-C-64159 TY II, Free Film
Effect of Exposure on Density
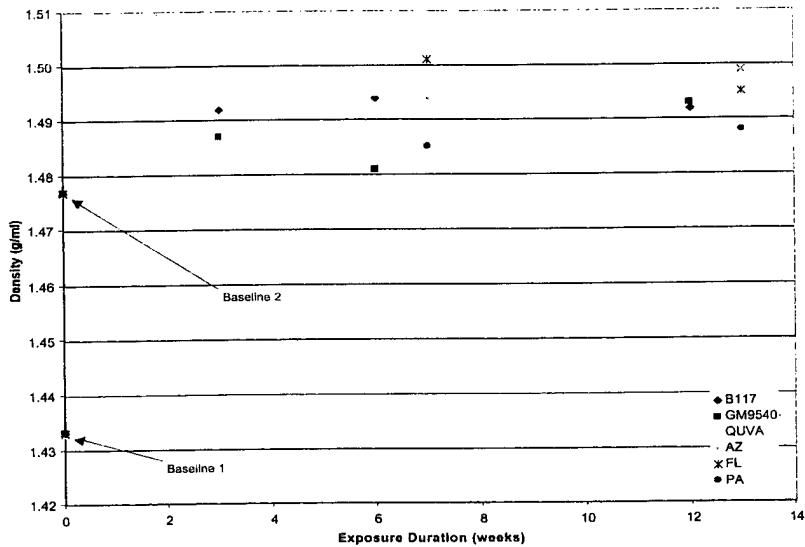
Figure 73: Scatter Plot, MIL-C-85285, Free Film
Effect of Exposure on Density

Figure 74: Scatter Plot, ZVOC TC, Free Film
Effect of Exposure on Density

Table 2: DMTA Data

CTG SYS	TOPCOAT	PRIMER	SUB	DATE (J.D.) APPLIC	DATE (J.D.) TEST	EXPOS TYPE (# day)	transition region α Tg (°C)	α tan δ (max)	β Tg (°C)	β tan δ (max)	glassy region E' (max) (Pa) 1x10⁸	E" (Pa) 1x10⁸	Temp (°C)	rubbery region E' (Pa) 1x10⁸	E' (min) (dyn/cm²) 1x10⁸	Temp (°C)	ve (mole/cm³) 1x10⁻³
A	46168	na	FF	3/16/00 (0076)	3/30/00 (0090)	RT (14)	72.1	0.7575	na	na	84.23	1.586	-0.1587	1.357	13.57	115.39	14.002273
A	46168	na	FF	3/16/00 (0076)	4/24/00 (0115)	RT (39)	65.9	0.7644	na	na	101.3	2.402	-0.2119	1.699	16.99	116.12	17.49992
A	46168	na	FF	3/16/00 (0076)	6/27/00 (0179)	RT (103)	62.4	0.7399	na	na	102.9	1.535	-28.04	1.579	15.79	122.51	16.00032
A	46168	na	FF	3/16/00 (0076)	5/30/00 (0151)	B3	76.505	0.5614	na	na	109.7		-39.8	2.067	20.67	170.76	18.66871
A	46168	na	FF	3/16/00 (0076)	6/20/00 (0172)	B6	77.952	0.585	na	na	94.59		-22.83	2.498	24.98	168.85	22.6589
A	46168	na	FF	3/16/00 (0076)	7/31/00 (0213)	B12	80.91	0.6183	na	na	99.44	1.74	-47.756	2.409	24.09	191.83	20.77166
A	46168	na	FF	3/16/00 (0076)	6/15/00 (0167)	G3	75.516	0.5702	na	na	105.9		-22.73	1.535	15.35	171.45	13.84228
A	46168	na	FF	3/16/00 (0076)	6/19/00 (0171)	G6	81.322	0.5239	na	na	104.5		-25.42	2.239	22.39	169.91	20.26097
A	46168	na	FF	3/16/00 (0076)	8/07/00 (0220)	G12	78.243	0.5399	na	na	115.2	1.44	-41.334	1.872	18.72	191.41	16.15596
A	46168	na	FF	3/16/00 (0076)	6/08/00 (0160)	Q3	73.4	0.522	na	na	83.91	1.523	-23.83	1.103	11.03	144.9	10.5783
A	46168	na	FF	3/16/00 (0076)	7/11/00 (0193)	Q6	72.67	0.405	na	na	112.4	2.188	-25.462	2.188	21.88	175.85	19.53753
A	46168	na	FF	3/16/00 (0076)	8/29/00 (0242)	Q12	73.358	0.3521	na	na	119.6	1.61	-43.515	2.43	24.3	194.87	20.81664
A	46168	na	FF	3/16/00 (0076)	7/14/00 (0196)	AZ7	69.279	0.695	na	na	94.03	1.149	-27.461	1.525	15.25	150.06	14.44717
A	46168	na	FF	3/16/00 (0076)	8/16/00 (0229)	AZ13	67.476	0.5418	na	na	107.7	1.553	-42.642	1.655	16.55	126.75	16.59263
A	46168	na	FF	3/16/00 (0076)	7/07/00 (0189)	FL7	75.202	0.6053	na	na	94.94	0.9337	~-28	1.62	16.2	159.96	14.99635
A	46168	na	FF	3/16/00 (0076)	9/05/00 (0249)	FL13	78.166	0.4924	na	na	96.03	0.9363	-43.259	1.849	18.49	166.11	16.87656
A	46168	na	FF	3/16/00 (0076)	6/26/00 (0178)	PA7	65.68	0.5717	na	na	108.4	1.676	~-20.5	1.813	18.13	131.17	17.978
A	46168	na	FF	3/16/00 (0076)	8/09/00 (0222)	PA13	70.97	0.612	na	na	104.3	1.438	-45.26	1.38	13.8	147.47	13.154
A	46168	na	FF	3/16/00 (0076)	3/29/00 (0089)	RT (13)	66.6	-0.42	undetectable	na	na	na	na	na	na	na	na
A	46168	na	FF	3/16/00 (0076)	4/26/00 (0117)	RT (41)	60.5	0.4669	undetectable	na	na	na	na	na	na	na	na
A	46168	53022	mesh	3/16/00 (0076)	5/31/00 (0152)	Q3	71.775	0.3359	undetectable	undetectable	na	na	na	na	na	na	na
A	46168	53022	mesh	3/16/00 (0076)	6/21/00 (0173)	Q6	73.747	0.3164	undetectable	undetectable	na	na	na	na	na	na	na
A	46168	53022	mesh	3/16/00 (0076)	8/01/00 (0214)	Q12	84.833	0.3058	undetectable	undetectable	na	na	na	na	na	na	na
A	46168	53022	mesh	3/16/00 (0076)	6/16/00 (0168)	G3	74.638	0.3403	undetectable	undetectable	na	na	na	na	na	na	na
A	46168	53022	mesh	3/16/00 (0076)	6/19/00 (0171)	G6	79.541	0.3532	undetectable	undetectable	na	na	na	na	na	na	na
A	46168	53022	mesh	3/16/00 (0076)	8/8/00 (0221)	G12	79.019	0.3688	undetectable	undetectable	na	na	na	na	na	na	na
A	46168	53022	mesh	3/16/00 (0076)	6/16/00 (0168)	B3	68.194	0.3457	undetectable	undetectable	na	na	na	na	na	na	na
A	46168	53022	mesh	3/16/00 (0076)	6/21/00 (0173)	B6	76.827	0.3617	undetectable	undetectable	na	na	na	na	na	na	na
A	46168	53022	mesh	3/16/00 (0076)	8/01/00 (0214)	B12	78.396	0.3804	undetectable	undetectable	na	na	na	na	na	na	na
A	46168	53022	mesh	3/16/00 (0076)	7/14/00 (0196)	AZ7	63.942	0.3653	undetectable	undetectable	na	na	na	na	na	na	na
A	46168	53022	mesh	3/16/00 (0076)	8/16/00 (0229)	AZ13	68.107	0.3669	undetectable	undetectable	na	na	na	na	na	na	na
A	46168	53022	mesh	3/16/00 (0076)	7/10/00 (0192)	FL7	74.506	0.324	undetectable	undetectable	na	na	na	na	na	na	na
A	46168	53022	mesh	3/16/00 (0076)	9/08/00 (0252)	FL13	78.521	0.337	undetectable	undetectable	na	na	na	na	na	na	na
A	46168	53022	mesh	3/16/00 (0076)	6/26/00 (0178)	PA7	65.426	0.3384	undetectable	undetectable	na	na	na	na	na	na	na
A	46168	53022	mesh	3/16/00 (0076)	8/10/00 (0223)	PA13	71.981	0.3251	undetectable	undetectable	na	na	na	na	na	na	na

Table 2: DMTA Data (cont.)

CTG SYS	TOPCOAT	PRIMER	SUB	DATE (J.D.) APPLIC	DATE (J.D.) TEST	EXPOS TYPE (# day)	transition region α T_n (°C)	α tan δ (max)	β T_n (°C)	β tan δ (max)	glassy region E' (max) (Pa) 1×10^8	E'' (Pa) 1×10^8	Temp (°C)	rubbery region (Pa) 1×10^8	E' (min) (dyn/cm²) 1×10^6	Temp (°C)	v_e (mole/cm³) 1×10^{-3}
B	64159 T2	na	FF	3/16/00 (0076)	4/25/00 (0116)	RT (40)	93	0.4178	na	na	31.82	1.267	-6.5137	0.63405	6.3405	167.33	5.771199
B	64159 T2	na	FF	3/16/00 (0076)	6/27/00 (0179)	RT (103)	94.6	0.3938	na	na	39.98	1.481	-20.204	0.7244	7.244	164.91	6.630001
B	64159 T2	na	FF	3/16/00 (0076)	5/30/00 (0151)	B3	100.59	0.3767	na	na	42.25		-45.325	0.5348	5.348	178.89	4.743329
B	64159 T2	na	FF	3/16/00 (0076)	6/20/00 (0172)	B6	101.92	0.3839	na	na	31.01		-27.154	0.4213	4.213	178.39	3.740795
B	64159 T2	na	FF	3/16/00 (0076)	7/31/00 (0213)	B12	100.54	0.3833	na	na	41.97	1.513	-42.221	0.5254	5.254	193.91	4.510099
B	64159 T2	na	FF	3/16/00 (0076)	6/15/00 (0167)	G3	100.43	0.3657	na	na	30.01	1.192	-20.443	0.5753	5.753	152.97	5.412915
B	64159 T2	na	FF	3/16/00 (0076)	6/19/00 (0171)	G6	100.24	0.3487	na	na	35.39		-26.681	0.5285	5.285	170.41	4.777067
B	64159 T2	na	FF	3/16/00 (0076)	8/7/00 (0220)	G12	98.325	0.3698	na	na	40.76	1.353	-48.041	0.4763	4.763	193.41	4.093001
B	64159 T2	na	FF	3/16/00 (0076)	6/08/00 (0160)	Q3	99.026	0.4344	na	na	35.01	1.155	-22.51	0.6277	6.277	172.36	5.648894
B	64159 T2	na	FF	3/16/00 (0076)	7/11/00 (0193)	Q6	99.192	0.4441	na	na	36.87	1.31	-22.62	0.5725	5.725	172.37	5.152014
B	64159 T2	na	FF	3/16/00 (0076)	8/29/00 (0242)	Q12	98.493	0.4903	na	na	39.54	1.283	-39.879	0.3852	3.852	98.493	4.155555
B	64159 T2	na	FF	3/16/00 (0076)	7/14/00 (0227)	AZ7	95.85	0.3796	na	na	35.76	1.417	-22.393	0.5637	5.637	174.45	5.049248
B	64159 T2	na	FF	3/16/00 (0076)	08/16/00 (0229)	AZ13	94.97	0.3993	na	na	36.34	1.209	-40.972	0.3896	3.896	190.88	3.366213
B	64159 T2	na	FF	3/16/00 (0076)	7/07/00 (0189)	FL7	98.171	0.3497	na	na	35.42	1.235	-22.362	0.4186	4.186	171.42	3.775094
B	64159 T2	na	FF	3/16/00 (0076)	09/05/00 (0249)	FL13	107.04	0.3759	na	na	41.71	1.424	-45.128	0.6141	6.141	191.78	5.295662
B	64159 T2	na	FF	3/16/00 (0076)	6/26/00 (0178)	PA7	96.85	0.3865	na	na	33.14	1.333	-27.37	0.5301	5.301	178.28	4.707996
B	64159 T2	na	FF	3/16/00 (0076)	08/09/00 (0222)	PA13	97.107	0.4037	na	na	37.46	1.222	-47.72	0.3686	3.686	196.42	3.147195
B	53030 T2	na	FF	3/16/00 (0076)	3/30/00 (0090)	RT (14)	83.6	~0.3	undetectable	undetectable	na	na	na	na	na	na	na
B	53030 T2	na	FF	3/16/00 (0076)	4/26/00 (0117)	RT (41)	78.2	0.3319	undetectable	undetectable	na	na	na	na	na	na	na
B	53030 T2	53030	mesh	3/16/00 (0076)	6/09/00 (0161)	Q3	106.04	0.3001	undetectable	undetectable	na	na	na	na	na	na	na
B	53030 T2	53030	mesh	3/16/00 (0076)	7/13/00 (0195)	Q6	101.53	0.3196	undetectable	undetectable	na	na	na	na	na	na	na
B	53030 T2	53030	mesh	3/16/00 (0076)	8/31/00 (0244)	Q12	107.44	0.369	undetectable	undetectable	na	na	na	na	na	na	na
B	53030 T2	53030	mesh	3/16/00 (0076)	6/16/00 (0168)	G3	107.84	0.3349	undetectable	undetectable	na	na	na	na	na	na	na
B	53030 T2	53030	mesh	3/16/00 (0076)	6/19/00 (0171)	G6	105.5	0.3631	undetectable	undetectable	na	na	na	na	na	na	na
B	53030 T2	53030	mesh	3/16/00 (0076)	8/08/00 (0221)	G12	104.59	0.3194	undetectable	undetectable	na	na	na	na	na	na	na
B	53030 T2	53030	mesh	3/16/00 (0076)	6/01/00 (0153)	B3	105.05	0.3548	undetectable	undetectable	na	na	na	na	na	na	na
B	53030 T2	53030	mesh	3/16/00 (0076)	6/21/00 (0173)	B6	106.13	0.3516	undetectable	undetectable	na	na	na	na	na	na	na
B	53030 T2	53030	mesh	3/16/00 (0076)	8/01/00 (0214)	B12	107.78	0.2934	undetectable	undetectable	na	na	na	na	na	na	na
B	53030 T2	53030	mesh	na	08/17/00 (0230)	AZ7	96.601	0.3553	undetectable	undetectable	omitted due to sample preparation error			na	na	na	na
B	53030 T2	53030	mesh	3/16/00 (0076)	na	AZ13	undetectable	undetectable	undetectable	undetectable	na	na	na	na	na	na	na
B	53030 T2	53030	mesh	3/16/00 (0076)	7/10/00 (0191)	FL7	104.11	0.3103	undetectable	undetectable	na	na	na	na	na	na	na
B	53030 T2	53030	mesh	3/16/00 (0076)	09/08/00 (0252)	FL13	105.73	0.2924	undetectable	undetectable	na	na	na	na	na	na	na
B	53030 T2	53030	mesh	3/16/00 (0076)	6/26/00 (0178)	PA7	102.48	0.3109	undetectable	undetectable	na	na	na	na	na	na	na
B	53030 T2	53030	mesh	3/16/00 (0076)	08/10/00 (0223)	PA13	102.51	0.3287	undetectable	undetectable	na	na	na	na	na	na	na

Table 2: DMTA Data (cont.)

Region groupings: columns $\alpha\,T_g$ through β tan δ (max) = **transition region**; E' (max), E", Temp = **glassy region**; E', E' (min), Temp, V_n = **rubbery region**.

CTG SYS	TOPCOAT	PRIMER	SUB	APPLIC DATE (J.D.)	TEST DATE (J.D.)	EXPOS TYPE (# day)	$\alpha\,T_g$ (°C)	α tan δ (max)	$\beta\,T_g$ (°C)	β tan δ (max)	E' (max) (Pa) 1×10^8	E" (Pa) 1×10^8	Temp (°C)	E' (Pa) 1×10^8	E' (min) (dyn/cm²) 1×10^8	Temp (°C)	V_n (mole/cm³) 1×10^{-3}
C	85285	na	FF	3/16/00 (0076)	4/7/00 (0098)	RT (22)	36.2	0.4873	na	na	48.063	0.96	-4.5	0.8917	8.917	164.47	8.169403
C	85285	na	FF	3/16/00 (0076)	4/25/00 (0116)	RT (40)	33.9	0.494	na	na	64.06	1.073	-50.324	0.8901	8.901	155.98	8.31608
C	85285	na	FF	3/16/00 (0076)	6/27/00 (0179)	RT (103)	29.7	0.4798	na	na	70.01	1.012	-49.163	0.639	6.39	145.04	6.126267
C	85285	na	FF	3/16/00 (0076)	5/30/00 (0151)	B3	32.582	0.4714	na	na	17.93	0.2116	-40.471	0.7177	7.177	145.92	6.866337
C	85285	na	FF	3/16/00 (0076)	6/20/00 (0172)	B6	31.902	0.4818	na	na	48.46	0.8414	-40.395	0.7303	7.303	143.07	7.034724
C	85285	na	FF	3/16/00 (0076)	7/31/00 (0213)	B12	32.651	0.5105	na	na	37.32	0.4678	-42.668	0.4147	4.147	180.94	3.661515
C	85285	na	FF	3/16/00 (0076)	6/15/00 (0167)	G3	32.823	0.4668	na	na	57.47	0.9333	-34.275	0.8856	8.856	142.47	8.54299
C	85285	na	FF	3/16/00 (0076)	6/19/00 (0171)	G6	31.365	0.4575	na	na	46.87	0.6918	-36.735	0.8815	8.815	115.66	9.089785
C	85285	na	FF	3/16/00 (0076)	8/08/00 (0221)	G12	31.849	0.4611	na	na	63.23	0.8013	-44.998	0.718	7.18	142.56	6.924728
C	85285	na	FF	3/16/00 (0076)	6/9/00 (0161)	Q3	29.489	0.4376	na	na	62.4	0.8159	-41.056	0.8115	8.115	147.46	7.735309
C	85285	na	FF	3/16/00 (0076)	7/13/00 (0194)	Q6	31.724	0.395	na	na	65.49	1.165	-43.467	0.7399	7.399	140.71	7.16784
C	85285	na	FF	3/16/00 (0076)	8/30/00 (0243)	Q12	35.719	0.3591	na	na	47.57	0.6636	-47.029	0.5265	5.265	172.91	6.732317
C	85285	na	FF	3/16/00 (0076)	7/14/00 (0196)	AZ7	32.699	0.4747	na	na	37.8	0.4732	-44.387	0.6858	6.858	132.38	6.780211
C	85285	na	FF	3/16/00 (0076)	08/16/00 (0229)	AZ13	30.521	0.4254	na	na	30.92	0.4503	-44.169	0.6227	6.227	141.1	6.026776
C	85285	na	FF	3/16/00 (0076)	7/14/00 (0196)	PA7	28.487	0.4599	na	na	54.2	0.8253	-32.905	0.6833	6.833	143.48	6.575512
C	85285	na	FF	3/16/00 (0076)	08/09/00 (0222)	PA13	32.017	0.4423	na	na	47.97	0.6668	-45.225	0.8136	8.136	139.57	7.903585
C	85286	na	FF	3/16/00 (0076)	7/07/00 (0189)	FL7	34.714	0.4533	na	na	63.14	0.8205	-47.52	0.9342	9.342	140.88	9.046421
C	85286	na	FF	3/16/00 (0076)	09/07/00 (0251)	FL13	38.397	0.4575	na	na	59.4	0.8747	-47.54	0.886	8.86	187.81	7.706181
C	85285	23377	mesh	3/16/00 (0076)	3/30/00 (0090)	RT (14)	77.1	0.404	26	0.07356	na	na	na	na	na	na	na
C	85285	23377	mesh	3/16/00 (0076)	4/26/00 (0117)	RT (41)	69.3	0.4032	21.6	0.0675	na	na	na	na	na	na	na
C	85285	23377	mesh	3/16/00 (0076)	6/16/00 (0168)	G3	79.905	0.3211	22.248	0.05807	na	na	na	na	na	na	na
C	85285	23377	mesh	3/16/00 (0076)	6/20/00 (0172)	G6	81.98	0.3298	15.718	0.04915	na	na	na	na	na	na	na
C	85285	23377	mesh	3/16/00 (0076)	8/09/00 (0222)	G12	84.682	0.3537	18.486	0.04621	na	na	na	na	na	na	na
C	85285	23377	mesh	3/16/00 (0076)	6/01/00 (0153)	B3	84.551	0.2983	18.064	0.06487	na	na	na	na	na	na	na
C	85285	23377	mesh	3/16/00 (0076)	6/21/00 (0173)	B6	85.297	0.264	18.123	0.06467	na	na	na	na	na	na	na
C	85285	23377	mesh	3/16/00 (0076)	8/01/00 (0214)	B12	91.524	0.3107	22.376	0.05117	na	na	na	na	na	na	na
C	85285	23377	mesh	3/16/00 (0076)	6/09/00 (0161)	Q3	76.05	0.3	17.541	0.05256	na	na	na	na	na	na	na
C	85285	23377	mesh	3/16/00 (0076)	7/13/00 (0195)	Q6	77.107	0.3237	18.956	0.05263	na	na	na	na	na	na	na
C	85285	23377	mesh	3/16/00 (0076)	8/31/00 (0244)	Q12	86.586	0.3358	19.494	0.04531	na	na	na	na	na	na	na
C	85285	23377	mesh	3/16/00 (0076)	7/14/00 (0196)	AZ7	73.39	0.3151	18.512	0.05807	na	na	na	na	na	na	na
C	85285	23377	mesh	3/16/00 (0076)	08/17/00 (0230)	AZ13	71.614	0.3097	18.073	0.05598	na	na	na	na	na	na	na
C	85285	23377	mesh	3/16/00 (0076)	7/10/00 (0192)	FL7	74.598	0.2826	23.538	0.05745	na	na	na	na	na	na	na
C	85285	23377	mesh	3/16/00 (0076)	09/08/00 (0252)	FL13	90.797	0.3242	24.809	0.05535	na	na	na	na	na	na	na
C	85285	23377	mesh	3/16/00 (0076)	6/27/00 (0179)	PA7	74.048	0.2938	20.954	0.06493	na	na	na	na	na	na	na
C	85285	23377	mesh	3/16/00 (0076)	08/11/00 (0224)	PA13	79.901	0.3108	19.44	0.05207	na	na	na	na	na	na	na

Table 2: DMTA Data (cont.)

CTG SYS	TOPCOAT	PRIMER	SUB	DATE (J.D.) APPLIC	DATE (J.D.) TEST	EXPOS TYPE (# day)	transition region αTg (°C)	α tan δ(max)	βTg (°C)	β tan δ(max)	glassy region E'(max) (Pa) 1x10^9	E" (Pa) 1x10^8	Temp (°C)	rubbery region E'(min) (Pa) 1x10^8	E'(min) (dyn/cm²) 1x10^8	Temp (°C)	ve (mole/cm³) 1x10^-3
D	ZVOC TC	na	FF	3/16/00 (0076)	4/25/00 (0116)	RT (40)	40.7	0.6383	na	na	43.44	0.8776	-38.345	0.3945	3.945	138	3.84694
D	ZVOC TC	na	FF	3/16/00 (0076)	6/28/00 (0180)	RT (104)	36.3	0.6145	na	na	46.63	0.735	-45.402	0.7548	7.548	130.69	7.493613
D	ZVOC TC	na	FF	3/16/00 (0076)	5/31/00 (0152)	B3	49.34	0.5786	na	na	42.39	0.7714	-43.667	0.4411	4.411	144.89	4.230463
D	ZVOC TC	na	FF	3/16/00 (0076)	6/21/00 (0173)	B6	40.014	0.5801	na	na	40.71	0.8417	-39.918	0.574	5.74	147.52	5.470652
D	ZVOC TC	na	FF	3/16/00 (0076)	7/31/00 (0213)	B12	40.392	0.5205	na	na	43.81	0.9949	-40.587	0.7102	7.102	187.35	6.183292
D	ZVOC TC	na	FF	3/16/00 (0076)	6/16/00 (0168)	G3	41.079	0.5529	na	na	39.96	0.8744	-38.851	0.5623	5.623	149.19	5.337951
D	ZVOC TC	na	FF	3/16/00 (0076)	6/19/00 (0171)	G6	39.386	0.5331	na	na	43.03	0.8771	-33.413	0.6777	6.777	149.14	6.434213
D	ZVOC TC	na	FF	3/16/00 (0076)	08/08/00 (0221)	G12	46.351	0.5224	na	na	37.95	1.57	-46.332	0.3685	3.685	183.83	3.233025
D	ZVOC TC	na	FF	3/16/00 (0076)	6/09/00 (0161)	Q3	36.168	0.6254	na	na	52.05	0.9265	-42.678	0.5663	5.663	124.2	5.714024
D	ZVOC TC	na	FF	3/16/00 (0076)	7/13/00 (0195)	Q6	40.58	0.5188	na	na	47.49	0.7946	-45.028	0.3677	3.677	145.09	3.524819
D	ZVOC TC	na	FF	3/16/00 (0076)	8/31/00 (0244)	Q12	47.626	0.4611	na	na	28.74	0.5503	-45.595	0.2613	2.613	168.9	2.369937
D	ZVOC TC	na	FF	3/16/00 (0076)	7/14/00 (0196)	AZ7	39.824	0.539	na	na	38.82	0.8335	-44.38	0.6068	6.068	147.59	5.782298
D	ZVOC TC	na	FF	3/16/00 (0076)	08/17/00 (0230)	AZ13	38.432	0.5064	na	na	41.37	0.7733	-44.592	0.6732	6.732	145.49	6.447214
D	ZVOC TC	na	FF	3/16/00 (0076)	7/10/00 (0192)	FL7	41.096	0.505	na	na	40.73	0.757	-43.695	0.5162	5.162	147.59	4.918956
D	ZVOC TC	na	FF	3/16/00 (0076)	09/07/00 (0251)	FL13	54.78	0.5145	na	na	49.85	0.9827	-45.415	0.9048	9.048	176.09	8.075007
D	ZVOC TC	85582 C-N	mesh	3/16/00 (0076)	3/30/00 (0090)	RT (14)	58.5	0.2888	undetectable	na	na	na	na	na	na	na	na
D	ZVOC TC	85582 C-N	mesh	3/16/00 (0076)	4/26/00 (0117)	RT (41)	55	~-0.35	~-30	~-0.14	na	na	na	na	na	na	na
D	ZVOC TC	na	FF	3/16/00 (0076)	6/26/00 (0178)	PA7	38.166	0.5563	na	na	48.93	0.8261	-42.613	0.8853	8.853	146.56	8.456874
D	ZVOC TC	na	FF	3/16/00 (0076)	08/10/00 (0223)	PA13	39.721	0.5107	na	na	45.16	0.7742	-43.957	0.7378	7.378	169.35	6.684887
D	ZVOC TC	85582 C-N	mesh	3/16/00 (0076)	6/16/00 (0168)	G3	82.985	0.3582	25.862	0.09819	na	na	na	na	na	na	na
D	ZVOC TC	85582 C-N	mesh	3/16/00 (0076)	6/20/00 (0172)	G6	81.815	0.3151	28.719	0.09349	na	na	na	na	na	na	na
D	ZVOC TC	85582 C-N	mesh	3/16/00 (0076)	08/09/00 (0222)	G12	80.302	0.3412	28.6	0.08232	na	na	na	na	na	na	na
D	ZVOC TC	85582 C-N	mesh	3/16/00 (0076)	6/01/00 (0153)	B3	83.553	0.3804	27.626	0.128	na	na	na	na	na	na	na
D	ZVOC TC	85582 C-N	mesh	3/16/00 (0076)	6/21/00 (0173)	B6	86.273	0.361	25.512	0.1144	na	na	na	na	na	na	na
D	ZVOC TC	85582 C-N	mesh	3/16/00 (0076)	8/02/00 (0215)	B12	88.206	0.3668	26.008	0.1191	na	na	na	na	na	na	na
D	85582 TC	85582 C-N	mesh	3/16/00 (0076)	6/12/00 (0164)	Q3	69.207	0.2986	24.931	0.09037	na	na	na	na	na	na	na
D	85582 TC	85582 C-N	mesh	3/16/00 (0076)	6/20/00 (0172)	Q6	73.433	0.2651	27.41	0.09117	na	na	na	na	na	na	na
D	85582 TC	85582 C-N	mesh	3/16/00 (0076)	9/1/00 (0245)	Q12	81.17	0.2817	30.37	0.0846	na	na	na	na	na	na	na
D	85582 TC	85582 C-N	mesh	3/16/00 (0076)	7/14/00 (0196)	AZ7	72.334	0.2913	22.955	0.0919	na	na	na	na	na	na	na
D	85582 TC	85582 C-N	mesh	3/16/00 (0076)	08/17/00 (0230)	AZ13	74.214	0.3242	27.506	0.07999	na	na	na	na	na	na	na
D	85582 TC	85582 C-N	mesh	3/16/00 (0076)	7/10/11 (0192)	FL7	79.032	0.3453	25.208	0.09118	na	na	na	na	na	na	na
D	85582 TC	85582 C-N	mesh	3/16/00 (0076)	09/08/00 (0252)	FL13	86.243	0.3045	31.485	0.0887	na	na	na	na	na	na	na
D	ZVOC TC	85582 C-N	mesh	3/16/00 (0076)	6/27/00 (0179)	PA7	76.124	0.3084	22.458	0.08758	na	na	na	na	na	na	na
D	ZVOC TC	85582 C-N	mesh	3/16/00 (0076)	08/11/00 (0224)	PA13	78.188	0.3236	24.641	0.09646	na	na	na	na	na	na	na

Table 3: Density Data

CTG SYS	TOPCOAT	SUB	EXPOS DUR* (wk)	DENSITY (g/ml) EXPOSURE TYPE					
				B117	GM9540	QUVA	AZ	FL	PA
A	MIL-C-46168	FF	0	1.927	1.927	1.927	1.927	1.927	1.927
A	MIL-C-46168	FF	0	1.922	1.922	1.922	1.922	1.922	1.922
A	MIL-C-46168	FF	3	1.927	1.920	1.926			
A	MIL-C-46168	FF	6	1.958	1.920	1.930			
A	MIL-C-46168	FF	7				1.929	1.937	1.948
A	MIL-C-46168	FF	12	1.950	1.946	1.942			
A	MIL-C-46168	FF	13				1.938	1.957	1.943
B	SERDP CARC	FF	0	1.433	1.433	1.433	1.433	1.433	1.433
B	SERDP CARC	FF	0	1.477	1.477	1.477	1.477	1.477	1.477
B	SERDP CARC	FF	3	1.492	1.487	1.483			
B	SERDP CARC	FF	6	1.494	1.481	1.495			
B	SERDP CARC	FF	7				1.494	1.501	1.485
B	SERDP CARC	FF	12	1.492	1.493	1.501			
B	SERDP CARC	FF	13				1.499	1.495	1.488
C	MIL-C-85285	FF	0	1.483	1.483	1.483	1.483	1.483	1.483
C	MIL-C-85285	FF	0	1.500	1.500	1.500	1.500	1.500	1.500
C	MIL-C-85285	FF	3	1.490	1.505	1.508			
C	MIL-C-85285	FF	6	1.490	1.506	1.519			
C	MIL-C-85285	FF	7				1.508	1.510	1.509
C	MIL-C-85285	FF	12	1.465	1.500	1.526			
C	MIL-C-85285	FF	13				1.507	1.510	1.509
D	ZVOC TC	FF	0	1.448	1.448	1.448	1.448	1.448	1.448
D	ZVOC TC	FF	0	1.458	1.458	1.458	1.458	1.458	1.458
D	ZVOC TC	FF	3	1.471	1.469	1.473			
D	ZVOC TC	FF	6	1.470	1.472	1.473			
D	ZVOC TC	FF	7				1.469	1.476	1.476
D	ZVOC TC	FF	12	1.471	1.474	1.479			
D	ZVOC TC	FF	13				1.474	1.476	1.474

SUB – Substrate
EXPOS DUR – Exposure Duration
Wk – Week
AZ – Arizona
FL – Florida
PA – Pennsylvannia

* Exposure duration represents only the continuous time in the designated accelerated laboratory or static field test. 0 week exposure duration represents 3 week at ambient laboratory conditions (baseline 1) or 7 week at ambient laboratory conditions (baseline 2).

NSWCCD DISTRIBUTION

Copies

3   Commander, Carderock Division
     Naval Surface Warfare Center
     9500 MacArthur Blvd.
     West Bethesda, MD 20817-5700

1   60   (Morton)
1   603   (Hardy)
1   603   (Rockwell)

Copies

16   Commanding Officer
     Carderock Division
     Naval Surface Warfare Center
     Naval Business Center
     Philadelphia, PA 19112-5083

1   62 (Eichinger)

1   624 (Steck/File)
4   624 (Patel)
4   624 (Pilgrim)
4   624 (Eng)
1   624 (Fayocavitz)
1   624 (Duckworth)

ARL DISTRIBUTION

Copies

5   Army Research Laboratory
     Weapons and Materials Research Directorate
     Attn: S. McKnight, Bldg 4600

US Navy

2   DTIC

1   Commander
     Naval Air Warfare Center, Aircraft Division
     Attn: Dr. K.J. Kovaleski
     Code 4341, Bldg 2188
     48066 Shaw Road Unit 5
     Putuxent River, MD 20670-1908

SERDP

1   SERDP Program Office
     901 N. Stuart Street, Suite 303
     Arlington, VA 22203
     Attn: Charles Pellerin